Epigenetic regulation of Wnt7b expression by the *cis*-acting long noncoding RNA lnc-Rewind in muscle stem cells.

Andrea Cipriano[1,#§], Martina Macino[1,2§], Giulia Buonaiuto[1], Tiziana Santini[3], Beatrice Biferali[1,2], Giovanna Peruzzi[3], Alessio Colantoni[1], Chiara Mozzetta[2]*, Monica Ballarino[1]*.

[1]Dept. of Biology and Biotechnology Charles Darwin, Sapienza University of Rome, P.le A. Moro 5, Rome, 00185, Italy; [2]Institute of Molecular Biology and Pathology (IBPM), National Research Council (CNR) at Sapienza University of Rome, Rome, 00185, Italy; [3]Center for Life Nano Science@Sapienza, Istituto Italiano di Tecnologia, Viale Regina Elena 291, Rome, 00161, Italy.

Running Head

Regulation of *Wnt7b* expression by a *cis*-acting lncRNA

Keywords

ncRNA, LncRNA, Epigenetics, Chromatin, muscle stem cells

*Corresponding authors

Monica Ballarino: monica.ballarino@uniroma1.it; Dept. of Biol. and Biotechnology "Charles Darwin", Sapienza University, P.le Aldo Moro 5, 00185 - Rome, Italy; +39-0649912201

Chiara Mozzetta: chiara.mozzetta@cnr.it; chiara.mozzetta@uniroma1.it; IBPM-CNR, P.le Aldo Moro 5, 00185 - Rome, Italy; +39-0649912326

§Co-first authors

#Present address

Andrea Cipriano: Dept. of Obstetrics & Gynecology, Stanford University, 94306 Stanford, CA, USA.

ABSTRACT

Skeletal muscle possesses an outstanding capacity to regenerate upon injury due to the adult muscle stem cells (MuSCs) activity. This ability requires the proper balance between MuSCs expansion and differentiation which is critical for muscle homeostasis and contributes, if deregulated, to muscle diseases. Here, we functionally characterize a novel chromatin-associated lncRNA, lnc-Rewind, which is expressed in murine MuSCs and conserved in human. We find that, in mouse, lnc-Rewind acts as an epigenetic regulator of MuSCs proliferation and expansion by influencing the expression of skeletal muscle genes and several components of the WNT (Wingless-INT) signalling pathway. Among them, we identified the nearby *Wnt7b* gene as a direct lnc-Rewind target. We show that lnc-Rewind interacts with the G9a histone lysine methyltransferase and mediates the *in cis* repression of *Wnt7b* by H3K9me2 deposition. Overall, these findings provide novel insights into the epigenetic regulation of adult muscle stem cells fate by lncRNAs.

38 **INTRODUCTION**

39 The transcriptional output of all organisms was recently found to be more complex than originally
40 imagined, as the majority of the genomic content is pervasively transcribed into a diverse range of
41 regulatory short and long non-protein coding RNAs (ncRNAs) (Abugessaisa et al., 2017; Carninci et
42 al., 2005; Cipriano and Ballarino, 2018). Among them, long noncoding RNAs (lncRNAs) are
43 operationally defined as transcripts longer than 200 nucleotides, which display little or no protein
44 coding potential. Since the initial discovery, numerous studies have demonstrated their contribution
45 to many biological processes, including pluripotency, cell differentiation and organisms development
46 (Ballarino et al., 2016; Fatica and Bozzoni, 2014). LncRNAs were demonstrated to regulate gene
47 expression at transcriptional, post-transcriptional or translational level. The function and the
48 mechanisms of action are different and primarily depend on their (nuclear or cytoplasmic) subcellular
49 localization (Carlevaro et al., 2019; Rinn and Chang, 2012; Ulitsky and Bartel, 2013). A large number
50 of lncRNAs localize inside the nucleus, either enriched on the chromatin or restricted to specific
51 nucleoplasmic foci (Engreitz et al., 2016; Sun et al., 2018). In this location, they have the capacity to
52 control the expression of neighbouring (*in cis*) or distant (*in trans*) genes by regulating their chromatin
53 environment and also acting as structural scaffolds of nuclear domains (Kopp and Mendell, 2018).
54 Among the most important functions proposed for *cis*-acting lncRNAs, there is their ability to
55 regulate transcription by recruiting repressing or activating epigenetic complexes to specific genomic
56 loci (Huarte et al., 2010; Maamar et al., 2013; McHugh et al., 2015; Wang et al., 2011).

57 In muscle, high-throughput transcriptome sequencing (RNA-seq) and differential expression analyses
58 have facilitated the discovery of several lncRNAs that are modulated during the different stages of
59 skeletal myogenesis and dysregulated in muscle disorders (Ballarino et al., 2016; Lu et al., 2013;
60 Zhao et al., 2019). Although the roles of these transcripts have been partially identified, we are still
61 far from a complete undestanding of their mechanisms of action. For instance, the knowledge of the
62 lncRNAs impact on adult muscle stem cells (MuSCs) biology is partial and only a few examples have
63 been characterized as functionally important. In the cytoplasm, the lncRNA Lnc-mg has been shown

64 to regulate MuSC differentiation by acting as a sponge for miR-125b (Zhu et al., 2017). In the nucleus,
65 the lncRNA Dum was found to promote satellite cells differentiation by recruiting Dnmts to the
66 developmental pluripotency-associated 2 (Dppa2) promoter, leading to CpG hypermethylation and
67 silencing (Wang et al., 2015). In mouse, we have previously identified several lncRNAs specifically
68 expressed during muscle *in vitro* differentiation and with either nuclear or cytoplasmic localization
69 (Ballarino et al., 2015). Among them, we found lnc-Rewind (**Re**pressor of **w**nt **ind**uction), a
70 chromatin-associated lncRNA conserved in human and expressed in proliferating C_2C_{12} myoblasts.
71 Here, we provide evidence on the role of lnc-Rewind in the epigenetic regulation of the WNT
72 (Wingless-INT) signalling in muscle cells. The Wnt transduction cascade has been demonstrated to
73 act as a conserved regulator of stem cell function *via* canonical (β-catenin) and non-canonical (planar
74 cell polarity [PCP] and calcium) signalling and dysregulation of its activity has been reported in
75 various developmental disorders and diseases (Nusse and Clevers, 2017). In the muscle stem cell
76 niche, Wnt signaling is key in coordinating MuSCs transitions from quiescence, proliferation,
77 commitment and differentiation (Brack et al., 2008; Eliazer et al., 2019; Lacour et al., 2017; Le Grand
78 et al., 2009; Parisi et al., 2015; Rudolf et al., 2016). Because of this central role, the Wnt pathway is
79 supervised by several mechanisms and different works have shown that lncRNAs can modulate it
80 both at transcriptional and post-transcriptional levels (Zarkou et al., 2018). Here, we provide evidence
81 that lnc-Rewind associates with the H3K9 methyltransferase G9a to regulate the deposition of
82 H3K9me2 *in cis* on the nearby *Wnt7b* gene. Our data show that lnc-Rewind expression is necessary
83 to maintain *Wnt7b* repressed and to allow MuSCs expansion and proper differentiation.
84

85 **RESULTS**

86 **Lnc-Rewind is a conserved chromatin-associated lncRNA expressed in satellite cells.**

87 In an attempt to uncover novel regulators of MuSCs activity, we decided to take advantage of the
88 atlas of newly discovered lncRNAs, that we previously identified as expressed in proliferating muscle
89 cells (Ballarino et al. 2015). Among them, we focused on lnc-Rewind, which is a lncRNA enriched

90 in proliferating myoblasts and overlapping pre-miR-let7c-2 (mmu-let-7c-2) and pre-miR-let7b
91 (mmu-let-7b) genomic loci (**Figure 1A**). An evolutionary conservation analysis performed by
92 examining FANTOM5 datasets (Noguchi et al., 2017) revealed the existence of a conserved
93 transcriptional start site localized in the syntenic locus (**Figure 1B**). RNA-seq (Legnini et al., 2017)
94 (**Figure 1B**) and semiquantitative (sq)RT-PCR analyses (**Figure S1A)** confirmed that also in
95 proliferating human myoblasts this region is actively transcribed to produce a transcript (hs_lnc-
96 Rewind) which displays an overall ~46% of (exonic and intronic) sequence identity (**Figure S1B**).
97 This is a relatively high value of conservation for lncRNAs (Pang et al., 2006) and adds functional
98 importance to the lnc-Rewind genomic locus.
99 To pinpoint possible roles of the murine transcript in myogenic differentiation we first assessed lnc-
100 Rewind expression and subcellular localization both in C_2C_{12} and FACS-isolated Muscle Stem Cells
101 (MuSCs) (**Figure S1C**) grown under proliferative and differentiating conditions. Proper myogenic
102 differentiation was confirmed by the expression of late muscle-specific genes such as myogenin
103 (*MyoG*) and muscle creatin kinase (*MCK*) (**Figure S1D**). Quantitative qRT-PCR analysis revealed
104 that lnc-Rewind expression is high in proliferating (GM) C_2C_{12} myoblasts and MuSCs and
105 significantly decreased in fully differentiated (DM) cells (**Figure 1C**). Subcellular fractionation of
106 cytoplasmic (Cyt) and nuclear (Nuc) fractions (**Figure 1D**) showed that the majority of the noncoding
107 transcript localises in the nuclear compartment of both proliferating myoblasts and MuSCs.
108 Accordingly, RNA fluorescence *in situ* hybridization (FISH) experiments performed both in MuSCs
109 (**Figures 1E-1F** and **S1E**) and C_2C_{12} (**Figure S1F**) cells confirmed the nuclear localization of lnc-
110 Rewind and further revealed its specific enrichment to discrete chromatin foci. Overall these results
111 point towards a role for lnc-Rewind in chromatin-based processes and suggest its possible
112 involvement in the epigenetic regulation of MuSCs homeostasis.

Figure 1

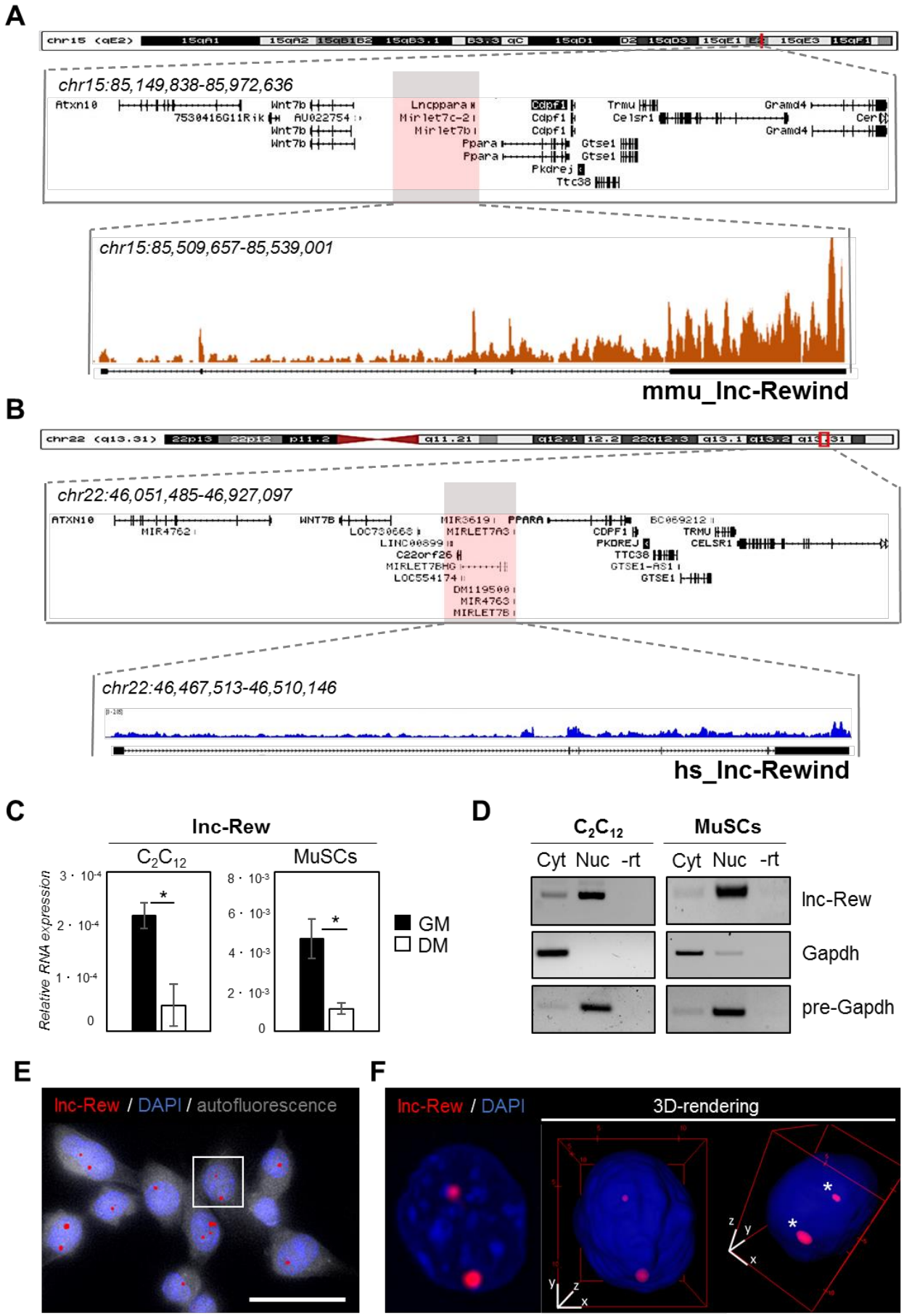
A
chr15:85,149,838-85,972,636
chr15:85,509,657-85,539,001
mmu_lnc-Rewind
B
chr22:46,051,485-46,927,097
chr22:46,467,513-46,510,146
hs_lnc-Rewind
C
lnc-Rew
C2C12
MuSCs
Relative RNA expression
GM
DM
D
C2C12
MuSCs
Cyt Nuc -rt
Cyt Nuc -rt
lnc-Rew
Gapdh
pre-Gapdh
E
lnc-Rew / DAPI / autofluorescence
F
lnc-Rew / DAPI
3D-rendering

113

Figure 1: Lnc-Rewind is a conserved chromatin-associated lncRNA expressed in satellite cells.

A) UCSC visualization showing the chromosome position and the genomic coordinates of lnc-Rewind (red box) in the mm9 mouse genome. The reads coverage from a RNA-Seq experiment performed in proliferating C_2C_{12} cells (GM) (Ballarino et al. 2015; GSE94498) together with the genomic structure of the lnc-Rewind locus are shown in the magnified box. **B)** UCSC visualization showing the chromosome position and the genomic coordinates of hs_lnc-Rewind (red box) in the hg19 human genome. The reads coverage from a RNA-Seq experiment performed in proliferating (MB) myoblast (Legnini et al., 2017; GSE70389) are shown below. **C)** Real-time RT-PCR (qRT-PCR) quantification of lnc-Rewind in myoblast (C_2C_{12}) and muscle satellite cells (MuSCs) in growth (GM) and differentiated (DM) conditions. Data represent the mean ± SEM of 3 biological replicates and were normalised on GAPDH mRNA. **D)** Semiquantitative RT-PCR (sqRT-PCR) quantification of lnc-Rewind in cytoplasmic (Cyt) and nuclear (Nuc) fractions from proliferating C2C12 and MuSCs. The quality of fractionation was tested with mature (GAPDH) and precursor (pre-GAPDH) RNAs. **E)** RNA-FISH analysis for lnc-Rewind RNA (red) in proliferating MuCS cell culture. Autofluorescence (grey) is shown with false color to visualize the cell body. DAPI, 4',6-diamidino-2-phenylindole (blue); Scale bar: 25 μm. **F)** Digital magnification and 3D-visualization of the square insert in panel E. Asterisks indicate lnc-Rewind RNA signals inside the nuclear volume. DAPI, 4',6-diamidino-2-phenylindole (blue). Data information: *P<0.05, paired Student's t-test.

114 **Lnc-Rewind regulates muscle system processes and MuSCs expansion.**

115 To gain insights into the functional role of lnc-Rewind and to identify the molecular pathways
116 involved in the regulation of MuSC, we performed a global transcriptional profiling on satellite cells
117 treated either with a mix of three different LNA GapmeRs against lnc-Rewind (GAP-REW) or with
118 a scramble control (GAP-SCR) (n=4) (**Figure S2A**, upper panel**)**. Under these conditions, we
119 obtained ~70% reduction of lnc-Rewind expression (**Figure S2A**, lower panel), which led to the
120 identification of a set of 1088 Differentially Expressed Genes (DEGs) ($p<0.05$, GAP-SCR *vs* GAP-
121 REW). Of these, 332 were upregulated and 756 downregulated in GAP-REW as compared to the
122 scramble condition (**Figure 2A** and **Table S1**). The PCA clustering analysis showed that the two
123 GAP-SCR and GAP-REW experimental groups displayed a clear different pattern of gene expression
124 since they occupy different regions of the PCA plot (**Figure S2B**). The prioritized DEGs list was then
125 subjected to Gene ontology (GO) term enrichment analysis (Biological process) to define functional
126 clusters. It emerged that DEGs were mostly associated with muscle cell physiology (skeletal muscle
127 contraction, P-value= 4.23E-6) (**Figure 2B** and **Figure S2C**). Of note, the analysis of lnc-Rewind
128 generated miRNAs (let7b and let7c2) revealed that although lnc-Rewind depletion results on their
129 concomitant downregulation (**Figure S2D**), none of the up-regulated transcripts that are also putative
130 let7b and let7c2 targets (~1% of the up-regulated genes) (**Figure S2E**), belong to any of the GO
131 enriched categories. This result emphasizes a specific and miRNA-independent role for lnc-Rewind.
132 Both "Muscle system process" (P-value= 3.45E) and "striated muscle contraction" (P-value= 4.63E-
133 7) were the most significantly enriched GO terms (**Figure S2C**). Of note, genes encoding for different
134 proteins involved in muscle contraction, such as myosins (i.e. *Myh8*, *Myh3*, *Myl1*) and troponins (i.e.
135 *Tnnt1*, *Tnnt2*) (**Figure 2C**) were downregulated. Accordingly, lnc-Rewind depleted MuSCs express
136 lower levels of MyHC proteins (**Figure 2D).** Morphological evaluation highlighted a decreased
137 number of MuSCs after lnc-Rewind depletion (**Figure S2F**), suggesting a primary defect in MuSCs
138 proliferation. This led us to hypothesize that the defects in myogenic capacity (**Figure 2C-2D and**
139 **S2F**) might result by a decreased cell density that normally leads to a lower rate of myogenic

140 differentiation. In line with this hypothesis, EdU incorporation experiments revealed a striking
141 reduction of proliferating MuSCs upon depletion of Lnc-Rewind (**Figure 2E**). Accordingly, the
142 *Ccnd3* gene encoding for Cyclin D3, a cyclin specifically involved in promoting transition from G1
143 to S phase, was significantly downregulated in lnc-Rewind-depleted MuSCs at both transcript (**Table**
144 **S1**) and protein levels (**Figure 2D**). In further support of this, MuSCs on single myofibers cultured
145 for 96 hours gave rise to a decreased percentage of proliferating ($Pax7^+/Ki67^+$) progeny upon *lnc-*
146 *Rewind* downregulation (**Figure 2F**). Moreover, quantification of the number of $Pax7^+$-derived
147 clusters (composed of more than 2 nuclei), pairs (composed of 2 nuclei) or single MuSCs within each
148 myofiber revealed a reduction of activated pairs and clusters upon lnc-Rewind depletion (**Figure 2G**),
149 suggesting a role for the lncRNA in sustaining MuSCs activation and expansion.

Figure 2

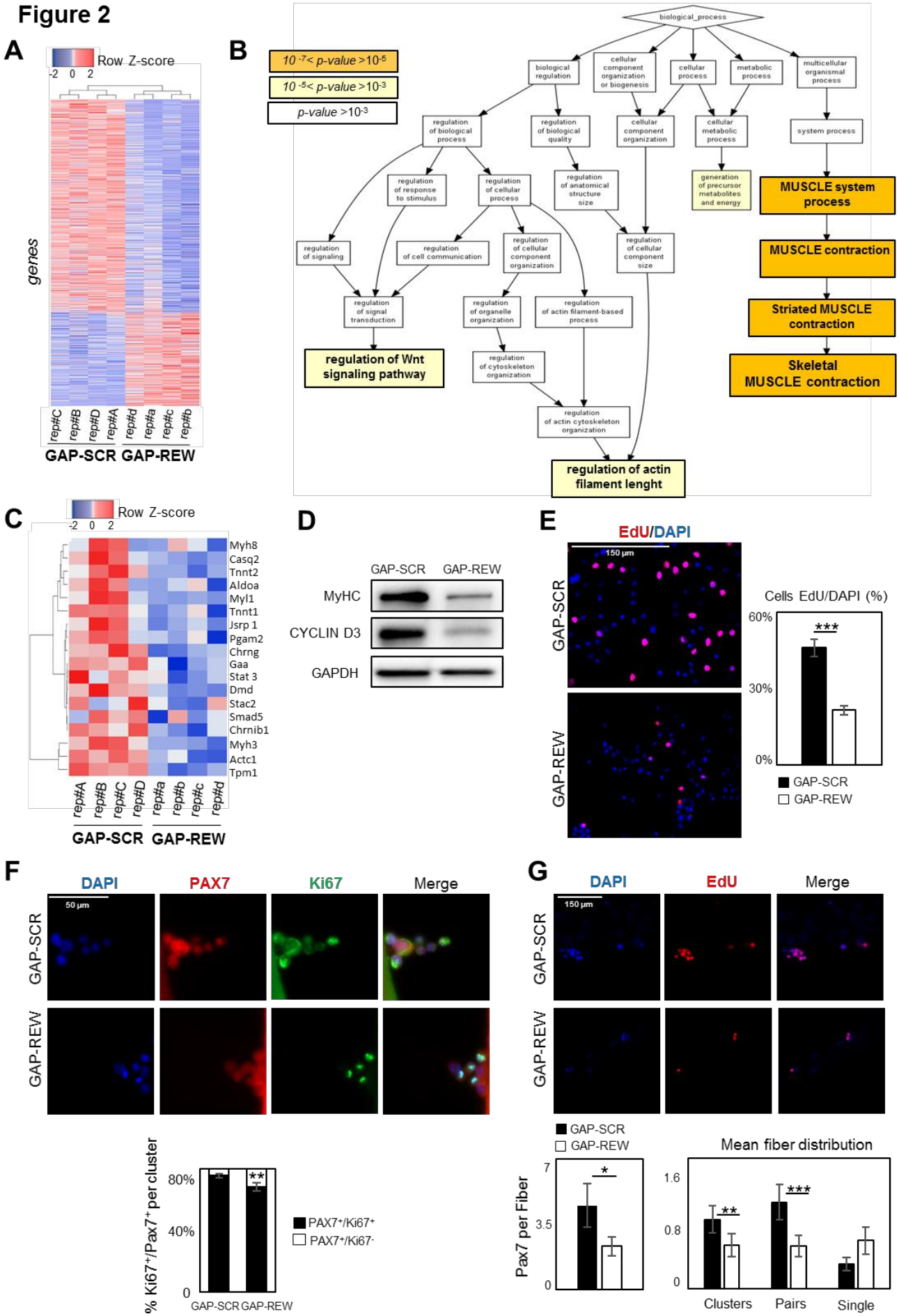
A
Row Z-score
-2 0 2
genes
rep#C rep#B rep#D rep#A rep#d rep#a rep#c rep#b
GAP-SCR GAP-REW
B
10 -7< p-value >10-5
10 -5< p-value >10-3
p-value >10-3
biological_process
biological regulation
cellular component organization or biogenesis
cellular process
metabolic process
multicellular organismal process
regulation of biological process
regulation of biological quality
cellular component organization
cellular metabolic process
system process
regulation of response to stimulus
regulation of cellular process
regulation of anatomical structure size
generation of precursor metabolites and energy
MUSCLE system process
regulation of signaling
regulation of cell communication
regulation of cellular component organization
regulation of cellular component size
MUSCLE contraction
regulation of signal transduction
regulation of organelle organization
regulation of actin filament-based process
Striated MUSCLE contraction
regulation of Wnt signaling pathway
regulation of cytoskeleton organization
Skeletal MUSCLE contraction
regulation of actin cytoskeleton organization
regulation of actin filament lenght
C
Row Z-score
-2 0 2
Myh8
Casq2
Tnnt2
Aldoa
Myl1
Tnnt1
Jsrp 1
Pgam2
Chrng
Gaa
Stat 3
Dmd
Stac2
Smad5
Chrnib1
Myh3
Actc1
Tpm1
rep#A rep#B rep#C rep#D rep#a rep#b rep#c rep#d
GAP-SCR GAP-REW
D
GAP-SCR GAP-REW
MyHC
CYCLIN D3
GAPDH
E
EdU/DAPI
150 µm
GAP-SCR
GAP-REW
Cells EdU/DAPI (%)
60%
30%
0%
***
GAP-SCR
GAP-REW
F
DAPI
PAX7
Ki67
Merge
50 µm
GAP-SCR
GAP-REW
% Ki67+/Pax7+ per cluster
80%
40%
0
**
PAX7+/Ki67+
PAX7+/Ki67-
GAP-SCR GAP-REW
G
DAPI
EdU
Merge
150 µm
GAP-SCR
GAP-REW
GAP-SCR
GAP-REW
Pax7 per Fiber
7
3.5
0
*
Mean fiber distribution
1.6
0.8
0
**
***
Clusters
Pairs
Single

150

Figure 2: Lnc-Rewind regulates muscle system processes and MuSCs expansion.

A) Heatmap represents hierarchical clustering performed on the common genes differentially expressed upon lnc-Rewind depletion in MuSC. The analysis was performed using Heatmapper webserver tool (Babicki et al., 2016). The expression levels for each gene correspond to their Z-score values. **B)** Gene Ontology (GO) enrichment analysis performed by GORILLA (Eden et al., 2009) in Biological Process for genes differentially expressed in response to lnc-Rewind depletion in MuSC. **C)** Heatmap represents hierarchical clustering performed on the common genes differentially expressed and belonging to the Skeletal Muscle contraction GO category (GO:0003009). The analysis was performed using the heatmapper webserver tool (Babicki et al., 2016). The expression levels for each gene correspond to their Z-score values. **D)** Western blot analysis performed on protein extracts from MuSCs treated with GAP-SCR or GAP-REW. **E)** Representative images of MuSCs treated with GAP-SCR and GAP-REW, incubated for 6 hours with EdU (red). Nuclei were visualized with DAPI (blu) (left panel) and the histogram shows the percentage of EdU positive cells on the total of DAPI positive cells. Data are graphed as mean ± SEM of 13 images with a total of more then 1000 cells per condition; N=1 mouse (right panel). **F)** Representative images of single muscle fibers treated with GAP-SCR or GAP-REW from Wt mice after 96 hours in culture, stained for Pax7 (red) and Ki67 (green). Nuclei were visualized with DAPI (blue) (upper panel); the histogram shows the percentage of $Pax7^{+}/Ki67^{-}$ cells on the total of $Pax7^{+}/Ki67^{+}$ cells per cluster (40 clusters per condition; n=5 mice) (lower panel). Data represent the mean ± SEM. **G)** Representative images of single muscle fibers treated with GAP-SCR or GAP-REW from Wt mice after 96 hours in culture, incubated for 24 hours with EdU (red). Nuclei were visualized with DAPI (blu) (upper panel); histograms represent the mean of clusters (n>2), pairs (n=2) and single cells $PAX7^{+}$ (n=1) per fiber. Data represent the mean ± SEM of 80 fibers per condition; n=5 mice (lower panel, right). The histogram (lower panel, left) shows the number of Pax7+ cells per fiber (50 fibers per condition; n=5 mice). Data information: statistical analysis was performed using unpaired Student's t-test: *P<0.05, **P<0.01, ***P<0.001.

151 ***Lnc-Rewind* and *Wnt7b* genes display opposite pattern of expression.**

152 Together with the muscle-specific genes, the "regulation of Wnt signaling pathway" term caught our
153 attention as it was represented by a significant subset of trancripts (P-value= 5.44E-4, **Figure S2C**).
154 Among them we found *Wnt7b*, which expression was found upregulated at both transcript (**Table S1**)
155 and protein level (**Figure S2G**), suggesting a role for *Lnc-Rewind* as a repressor of *Wnt7b* expression.
156 Intriguingly, *Wnt7b* transcriptional locus localizes only100 kb upstream *lnc-Rewind* gene (**Figure**
157 **3A**). Their anticorrelated expression together with the lncRNA chromatin enrichment (**Figure 1D**)
158 and the proximity between the two transcription loci, led us to hypothesize that lnc-Rewind might
159 have a direct, *in cis*-regulatory role on *Wnt7b* transcription. A first clue in favour of such hypothesis
160 came from FANTOM5 Cap Analysis Gene Expression (CAGE) profiles of mouse samples, available
161 on ZENBU genome browser (Noguchi et al., 2017). Indeed, the inspection of the Transcriptional Start
162 Site (TSS) usage among all the available samples (n=1196) revealed a distinctive anti-correlated
163 expression of murine lnc-Rewind and Wnt7b transcripts (**Figure 3B**, left panels). In contrast, the
164 expression of the other lnc-Rewind-neighbouring genes, such as Cdpf1 and Atxn10, displayed no
165 specific expression correlation (**Figure 3B**, right panels). Of note, among the different genes analysed
166 in proximity to *Lnc-Rewind* gene, Wnt7b was the only gene significantly upregulated upon the
167 lncRNA depletion (**Figure 3C-D)** with a concomitant increase in WNTb protein levels (**Figure S2G**).
168 Although the function of WNT7b has been studied in different cell types and developmental processes
169 (Chen et al., 2014; Wang et al., 2005), the involvement of this ligand in muscle biology is still rather
170 unexplored. The fact that in MuSCs, *Wnt7b* gene is mantained at very low levels and that it is latest
171 Wnt ligand induced after muscle injury (Polesskaya et al., 2003), suggests that the role of WNT7b in
172 muscle might be limited to late stages of myogenic differentiation and implies the necessity to keep
173 it repressed in MuSCs. Our results candidates Lnc-Rewind as a regulator of *Wnt7b* repression in
174 muscle and prompted us towards the study of the underlying mechanism by which this regulation
175 occurs.

Figure 3

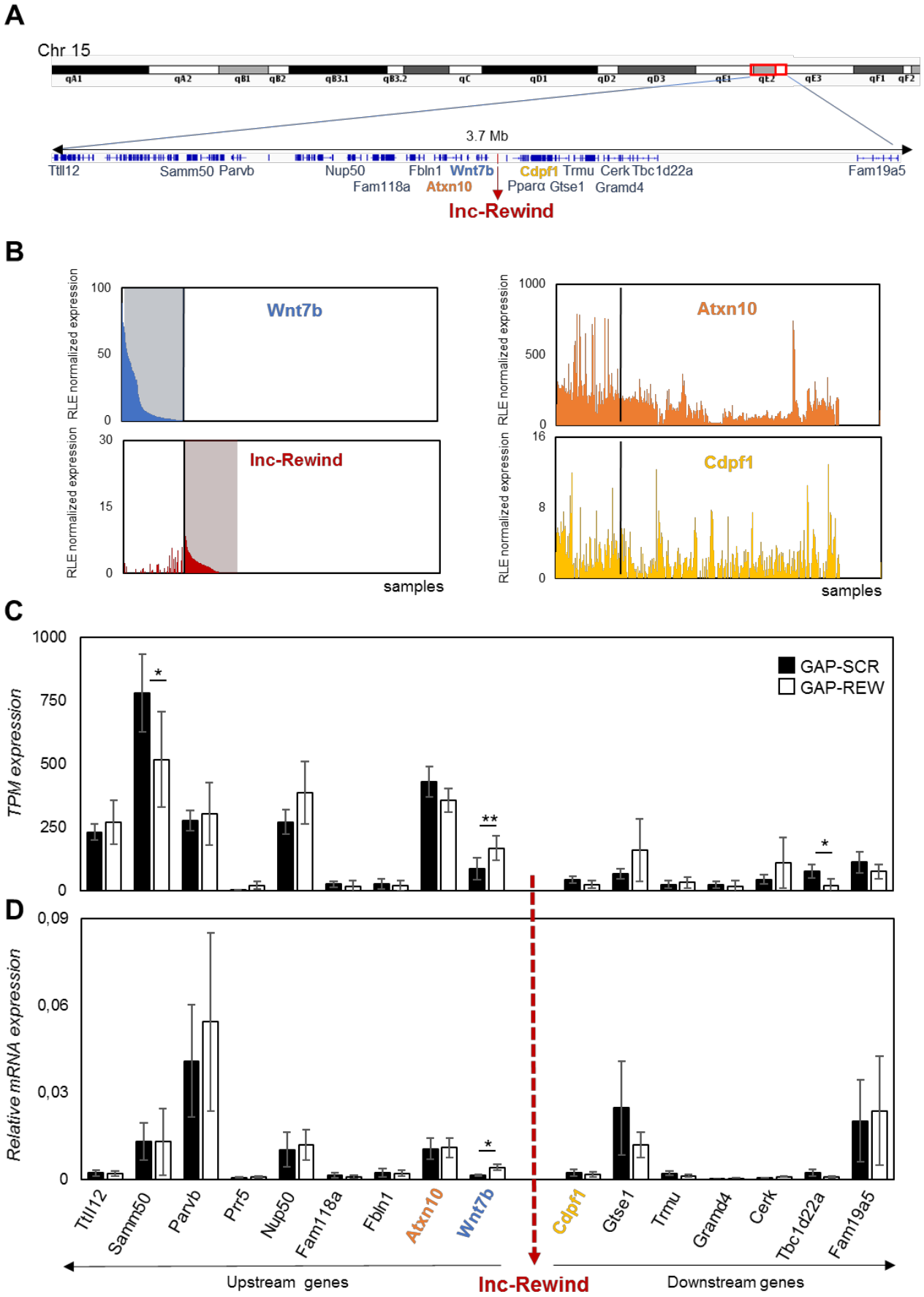
A
Chr 15
qA1
qA2
qB1
qB2
qB3.1
qB3.2
qC
qD1
qD2
qD3
qE1
qE2
qE3
qF1
qF2
3.7 Mb
Ttll12
Samm50
Parvb
Nup50
Fbln1
Wnt7b
Cdpf1
Trmu
Cerk
Tbc1d22a
Fam19a5
Fam118a
Atxn10
Pparα
Gtse1
Gramd4
Inc-Rewind
B
RLE normalized expression
Wnt7b
Inc-Rewind
Atxn10
Cdpf1
samples
C
TPM expression
GAP-SCR
GAP-REW
D
Relative mRNA expression
Ttll12
Samm50
Parvb
Prr5
Nup50
Fam118a
Fbln1
Atxn10
Wnt7b
Cdpf1
Gtse1
Trmu
Gramd4
Cerk
Tbc1d22a
Fam19a5
Upstream genes
Inc-Rewind
Downstream genes

176

Figure 3: *Lnc-Rewind* and *Wnt7b* genes display opposite pattern of expression

A) Schematic UCSC visualization showing the chromosome position and the lnc-Rewind neighbouring genes. **B)** TSS usage analysis of Wnt7b, lnc-Rewind, Atxn10 and Cdpf1 performed by using FANTOM5 (Phase1 and 2) CAGE datasets. Each bar represents the relative logarithmic expression (rle) of the Tag Per Million (TPM) values of the TSS of each gene in one sample (1196 samples). The order of the samples is the same in each of the histograms. **C)** TPM expression (from RNA-seq analysis) of lnc-Rewind neighbouring genes in GAP-SCR *versus* GAP-REW treated MuSCs. TPM expression values are presented as an average±SD of 4 biological replicates. **D)** qRT-PCR quantification of lnc-Rewind neighbouring genes in GAP-SCR *versus* GAP-REW treated MuSCs. Data were normalized to GAPDH mRNA and represent the average ±SEM of 4 biological replicates. Data information: *P<0.05, **P<0.01, paired Student's t-test.

177 **Lnc-Rewind directly interacts with the methyltransferase G9a and mediates specific *in-cis***
178 **repression of *Wnt7b* in MuSCs.**
179 The above results suggest that Lnc-Rewind exerts a repressive role on Wnt7b expression, Several
180 works accumulated so far indicate that most of the *cis*-acting chromatin-associated lncRNAs function
181 occurs by recruiting and guiding chromatin modifiers to target genes (Batista and Chang, 2013;
182 Guttman and Rinn, 2012; Khalil et al., 2009; Rinn and Chang, 2012). In light of our data showing a
183 negative correlation of *Wnt7b* expression by Lnc-Rewind, we focused our attention on the two most
184 known repressive lysine methyltransferases, EZH2 and G9a, which catalyse the deposition of
185 H3K27me3 and H3K9me1/2 on target genes, respectively (Mozzetta et al., 2015). Both EZH2
186 (Caretti et al., 2004) and G9a (Ling et al., 2012) are mostly expressed in proliferating MuSCs and
187 become downregulated during muscle differentiation (**Figure S3A**), similarly to Lnc-Rewind.
188 Moreover, both Ezh2 (Rinn et al., 2007; Zhao et al., 2008) and G9a (Nagano et al., 2008; Pandey et
189 al., 2008) have been previously reported to be recruited to specific genomic loci trough the interaction
190 with different lncRNAs. Thus, we hypothesized that in proliferating myoblasts Lnc-Rewind might
191 interact with Ezh2 and/or G9a repressive complexes to tether them on *Wnt7b* genomic locus.
192 Therefore, we performed RNA immunoprecipitation (RIP) analysis in proliferating C_2C_{12} cells using
193 antibodies against G9a and Ezh2. We observed that, although both G9a and Ezh2 were successfully
194 immunoprecipitated (**Figure 4A**, upper panel**)**, Lnc-Rewind transcript was efficiently retrieved only
195 in the G9a native RNA immunoprecipitation (IP), while it was almost undetectable in Ezh2 IP
196 (**Figure 4A**, lower panel**)**. The specificity of the interaction between Lnc-Rewind with G9a, was
197 further confirmed through Crosslinked Immunoprecipitation (CLIP) assay (**Figure 4B)**. Indeed, we
198 found that lnc-Rewind was specifically enriched in the G9a immunoprecipitation if compared to the
199 GAPDH negative control. To note, the levels of RNA obtained in the specific IP fraction were the
200 same of the Kcnq1ot1 lncRNA which was previously demonstrated to be physically associated with
201 G9a (Pandey et al., 2008).

202 In order to test whether Lnc-Rewind/G9a interaction has a role for the deposition of H3K9me2 mark
203 on *Wnt7b* containing regions, we performed a chromatin immunoprecipitation (ChIP) assay for
204 H3K9me2 in scramble and Lnc-Rewind gapmer transfected MuSCs. We analysed different regions
205 upstream *Wnt7b* TSS (**Figure 4C**, upper panel) and quantification of H3K9me2 enrichment led to the
206 identification of three regions (named G9a/91, G9a/93 and G9a/94) in which H3K9me2 levels
207 decreased upon Lnc-Rewind knockdown, compared to the SCR control (**Figure 4C**, lower panel).
208 Taken together, these results support a mechanism of action through which in MuSCs Lnc-Rewind
209 represses *Wnt7b* gene transcription by mediating the specific G9a-dependent H3K9me2 deposition
210 on its locus (**Figure 4D)**.

Figure 4

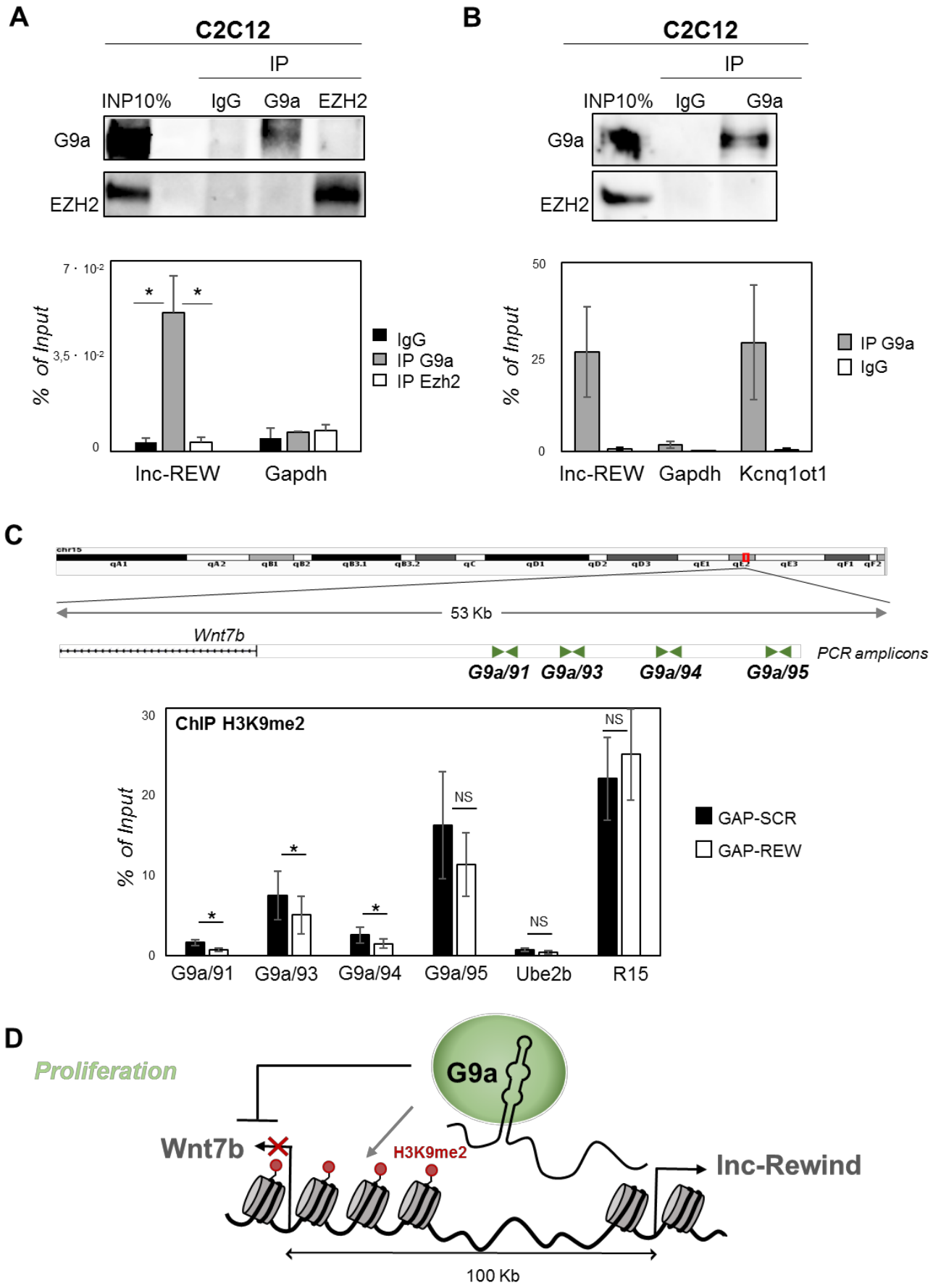
A
C2C12
IP
INP10%
IgG
G9a
EZH2
G9a
EZH2
% of Input
7 · 10-2
3,5 · 10-2
0
IgG
IP G9a
IP Ezh2
lnc-REW
Gapdh
B
C2C12
IP
INP10%
IgG
G9a
G9a
EZH2
% of Input
50
25
0
IP G9a
IgG
lnc-REW
Gapdh
Kcnq1ot1
C
53 Kb
Wnt7b
PCR amplicons
G9a/91
G9a/93
G9a/94
G9a/95
ChIP H3K9me2
% of Input
30
20
10
0
NS
GAP-SCR
GAP-REW
G9a/91
G9a/93
G9a/94
G9a/95
Ube2b
R15
D
Proliferation
G9a
Wnt7b
H3K9me2
lnc-Rewind
100 Kb

211

Figure 4: Lnc-Rewind directly interacts with the methyltransferase G9a and mediates specific *in-cis* repression of *Wnt7b*.

A) G9A and EZH2 native RNA immunoprecipitation (RIP) performed on nuclear extracts of C_2C_{12} proliferating myoblasts. Data represent mean ±SEM of 4 biological replicates. Western blot analysis of G9A and EZH2 (upper panel) and qRT-PCR quantification of lnc-Rewind recovery (lower panel) are shown. Gapdh RNA serves as negative control. **B)** G9a Cross-linked RNA immunoprecipitation (CLIP) performed on nuclear extracts of C_2C_{12} proliferating myoblasts. Data represent mean ±SEM of 3 biological replicates. Western blot analysis of G9A (upper panel) and qRT-PCR quantification of lnc-Rewind recovery (lower panel) are shown. Gapdh RNA and EZH2 protein serve as negative controls; Kcnq1ot RNA was used as positive control. **C)** A zoom in into the genomic regions upstream *Wnt7b* gene. Amplicons used to check the H3K9me2 epigenetic mark are shown. Chromatin immunoprecipitation (ChIP) of H3K9me2, performed in Wt MuSCs upon lnc-Rewind downregulation; MuSCs transfected with scrambled (GAP-SCR) gapmers have been used as control. Enrichment is represented as percentage of input DNA (% input). Ube2b and R15 genomic regions were used as negative and positive control, respectively. The graph shows the averaged value derived from n=6 independent experiments. **D)** Proposed model for the murine lnc-Rewind mode of action in muscle cells. In proliferating myoblasts, lnc-Rewind is expressed and guide the silencing methyltransferase G9a on *Wnt7b* promoter to repress its transcription. Data information: *P<0.05, paired Student's t-test.

212 **DISCUSSION**

213 Wnt signalling represents one of the pathways that has a major role in myogenesis as it is essential
214 for proper MuSCs self-renewal and differentiation (von Maltzahn et al., 2012). A correct timing of
215 Wnt signalling activation is crucial to obtain proper tissue repair and its aberrant activity causes a
216 wide range of pathologies (Nusse and Clevers, 2017) Thus, it is not surprising that Wnt pathway is
217 under a strict positive and negative multi-layered regulation. Recent studies show that long noncoding
218 RNAs can modulate Wnt pathway by affecting gene expression through different mechanisms, from
219 transcriptional to post-transcriptional level (Ong et al., 2017; Shen et al., 2017; Zarkou et al., 2018)
220 For example, lncRNAs were found interacting with transcription factors (Di Cecilia et al. 2016) and
221 chromatin modifiers (Hu et al., 2015) altering Wnt signaling pathway in different tissues and in
222 cancer. In this study we discovered that lncRNAs-mediated regulation plays a role in modulating Wnt
223 pathway in muscle stem cells. Taking advantage of a newly discovered atlas of not annotated muscle-
224 specific lncRNAs (Ballarino et al., 2015), we decided to focus our attention on Lnc-Rewind for the
225 following reasons: i) an orthologue transcript, hs_lnc-Rewind, with high level of sequence identity is
226 expressed by human myoblasts (**Figure 1B and S1A-B**); ii) lnc-Rewind is associated and retained to
227 chromatin (**Figue 1D-F**); iii) it is in genomic proximity to *Wnt7b* locus (**Figure 3A**) and iv) its knock-
228 down induces upregulation of Wnt7b in MuSCs (**Figure 3C and S2G**). These observations led us
229 hypothesize a Lnc-Rewind-mediated *in-cis* repression for *Wnt7b* gene. Of note, by analyzing the
230 expression of surrounding genes within Lnc-Rewind genomic region, *Wnt7b* is the only gene to be
231 significantly up-regulated by Lnc-Rewind depletion (**Figure 3C-D**). Moreover, we show that Lnc-
232 Rewind and *Wnt7b* expression are anti-correlated in other cell types (**Figure 3B**), suggesting that the
233 repressive action of Lnc-Rewind on *Wnt7b* locus could have a more general role, not only in satellite
234 cells.

235 It is well-accepted that the majority of the *cis*-acting chromatin-associated lncRNAs function by
236 recruiting and targeting chromatin modifiers to specific genes (Batista and Chang, 2013; Guttman
237 and Rinn, 2012; Khalil et al., 2009; Rinn and Chang, 2012). In light of the evidence that Lnc-Rewind

238 promotes *Wnt7b* repression, we decided to investigate the involvement of the two major repressive
239 histone modifiers, Ezh2 and G9a, in mediating such Lnc-Rewind-dependent silencing. Notably, by
240 performing two different biochemical approaches (RIP and CLIP), we found that only G9a,
241 specifically interacts with Lnc-Rewind (**Figure 4A-B**). This strongly suggests that this histone H3K9
242 lysine methyltransferase (KMT) might be specifically tethered on *Wnt7b* genomic locus by Lnc-
243 Rewind to mediate its transcriptional repression. In support to this idea, through H3K9me2 ChIP
244 experiments here we provide evidence that different regions upstream *Wnt7b* locus are enriched in
245 the G9a-deposited histone mark in proliferating MuSCs and that H3K9me2 levels on these regions
246 significantly decrease upon lnc-Rewind knockdown (**Figure 4C**). Finally, expression profiling of
247 Lnc-Rewind-depleted MuSCs strongly confirmed a functional role for this novel lncRNA as a
248 modulator of Wnt signalling (**Figure 2B**), myogenic capacity (**Figure 2B-C-D** and **S2F**) and MuSCs
249 expansion (**Figure 2E-F-G**).
250 A correct timing and magnitude of Wnt signalling activation is essential to maintain functionl MuSCs.
251 For instance, it has been shown that low β-catenin activity is fundamental during early phases of
252 muscle regeneration to allow MuSCs activation and subsequent differentiation (Figeac and Zammit,
253 2015; Parisi et al., 2015). Accordingly, satellite cells isolated from mice with constitutive active
254 Wnt/β-catenin signalling display an early growth arrest and premature differentiation (Rudolf et al.,
255 2016). All these data point out that the cell environment, together with the timing and the proper
256 activation of Wnt signaling pathway is foundamental for muscle homeostasis. Here we show that
257 aberrant, cell-autonomous activation of Wnt7b expression upon Lnc-Rewind depletion causes defects
258 in MuSCs expansion and activation (**Figure 2E-F-G**), emphasizing that Lnc-Rewind-mediated
259 repression of *Wnt7b* is key in ensuring MuSCs activity. This is nicely supported by a previous study
260 demonstrating that, in the cytoplasm, a Wnt7b/lncRNA circuitry controls the proliferation of C_2C_{12}
261 myoblasts. Specifically, Lu and colleagues demonstrated that the YY1-associated muscle lincRNA
262 (Yam-1) inhibits skeletal myogenesis through modulation of miR-715 expression, which in turn
263 targets Wnt7b mRNA (Lu et al., 2013). In sum, our results support a mechanism of action through

264 which Lnc-Rewind mediates G9a recruitment on *Wnt7b* locus to silence it through the deposition of
265 the repressive mark H3K9me2 during the proliferation phase of satellite cells (**Figure 4D**), thus
266 providing unique insights on the contribution of nuclear-enriched lncRNAs in myogenesis.
267

268 **DATA AND SOFTWARE AVAILABILITY**

269 Data that support the findings of this study have been deposited in GEO with the primary accession
270 code GSE141396
271 https://www.ncbi.nlm.nih.gov/geo/query/acc.cgi?acc=GSE141396;
272 GEO reviewer token: mlqfamksbrirvip
273

274 **SUPPLEMENTAL INFORMATION**

275 Table S1.
276

277 **ACKNOWLEDGMENTS**

278 This work was partially supported by grants from Sapienza University (prot. RM11715C7C8176C1
279 and RM11916B7A39DCE5) and FFABR Anvur (2017) to M.B.. C.M. laboratory is funded by Italian
280 Ministry of University and Research (SIR, Scientific Independence of Young Researcher n.
281 RBSI14QMG0), Italian Association for Cancer Research (AIRC; MyFIRST grant n.18993), AFM-
282 Telethon (#22489) and the CNCCS (Collection of National Chemical Compounds and Screening
283 Center), LIFE2020-Regione Lazio.
284

285 **AUTHOR CONTRIBUTIONS**

286 C.M. and M.B. conceived, supervised the project and wrote the manuscript. A.C. performed the
287 cellular and molecular analyses in C_2C_{12} cells, RNA-seq analysis, TSS usage, Gene Onthologies
288 studies, ChIP experiments and the statistical analyses; M.M. performed the cellular and molecular
289 experiments carried out on MuSCs and myofibers, RIP and CLIP on C_2C_{12}; B.B. contributed to the

290 cellular experiments on MuSCs and myofibers. G.P. perfomed FACS isolation of MuSCs. T.S.
291 performed RNA-FISH; G.B. contributed to the molecular analyses performed in C_2C_{12} and MuSCs
292 cells; Al. Col. performed the bioinformatic analysis of the human myoblast RNA-seq. All authors
293 discussed results, reviewed and edited the manuscript.
294
295 **DECLARATION OF INTERESTS**
296 The authors declare no competing financial interests.
297
298 **FIGURE LEGEND**
299 **Figure 1: Lnc-Rewind is a conserved chromatin-associated lncRNA expressed in satellite cells.**
300 **A)** UCSC visualization showing the chromosome position and the genomic coordinates of lnc-
301 Rewind (red box) in the mm9 mouse genome. The reads coverage from a RNA-Seq experiment
302 performed in proliferating C_2C_{12} cells (GM) (Ballarino et al. 2015; GSE94498) together with the
303 genomic structure of the lnc-Rewind locus are shown in the magnified box. **B)** UCSC visualization
304 showing the chromosome position and the genomic coordinates of hs_lnc-Rewind (red box) in the
305 hg19 human genome. The reads coverage from a RNA-Seq experiment performed in proliferating
306 (MB) myoblast (Legnini et al., 2017; GSE70389) are shown below. **C)** Real-time RT-PCR (qRT-
307 PCR) quantification of lnc-Rewind in myoblast (C_2C_{12}) and muscle satellite cells (MuSCs) in growth
308 (GM) and differentiated (DM) conditions. Data represent the mean $\pm$ SEM of 3 biological replicates
309 and were normalised on GAPDH mRNA. **D)** Semiquantitative RT-PCR (sqRT-PCR) quantification
310 of lnc-Rewind in cytoplasmic (Cyt) and nuclear (Nuc) fractions from proliferating C2C12 and
311 MuSCs. The quality of fractionation was tested with mature (GAPDH) and precursor (pre-GAPDH)
312 RNAs. **E)** RNA-FISH analysis for lnc-Rewind RNA (red) in proliferating MuCS cell culture.
313 Autofluorescence (grey) is shown with false color to visualize the cell body. DAPI, 4',6-diamidino-
314 2-phenylindole (blue); Scale bar: 25 μm. **F)** Digital magnification and 3D-visualization of the square
315 insert in panel E. Asterisks indicate lnc-Rewind RNA signals inside the nuclear volume. DAPI, 4',6-

316 diamidino-2-phenylindole (blue). Data information: *P<0.05, paired Student's t-test.

317

318 **Figure 2: Lnc-Rewind regulates muscle system processes and MuSCs expansion.**

319 **A)** Heatmap represents hierarchical clustering performed on the common genes differentially
320 expressed upon lnc-Rewind depletion in MuSC. The analysis was performed using Heatmapper
321 webserver tool (Babicki et al., 2016). The expression levels for each gene correspond to their Z-score
322 values. **B)** Gene Ontology (GO) enrichment analysis performed by GORILLA (Eden et al., 2009) in
323 Biological Process for genes differentially expressed in response to lnc-Rewind depletion in MuSC.
324 **C)** Heatmap represents hierarchical clustering performed on the common genes differentially
325 expressed and belonging to the Skeletal Muscle contraction GO category (GO:0003009). The analysis
326 was performed using the heatmapper webserver tool (Babicki et al., 2016). The expression levels for
327 each gene correspond to their Z-score values. **D)** Western blot analysis performed on protein extracts
328 from MuSCs treated with GAP-SCR or GAP-REW. **E)** Representative images of MuSCs treated with
329 GAP-SCR and GAP-REW, incubated for 6 hours with EdU (red). Nuclei were visualized with DAPI
330 (blu) (left panel) and the histogram shows the percentage of EdU positive cells on the total of DAPI
331 positive cells. Data are graphed as mean ± SEM of 13 images with a total of more then 1000 cells per
332 condition; N=1 mouse (right panel). **F)** Representative images of single muscle fibers treated with
333 GAP-SCR or GAP-REW from Wt mice after 96 hours in culture, stained for Pax7 (red) and Ki67
334 (green). Nuclei were visualized with DAPI (blue) (upper panel); the histogram shows the percentage
335 of $Pax7^{+}/Ki67^{-}$ cells on the total of $Pax7^{+}/Ki67^{+}$ cells per cluster (40 clusters per condition; n=5 mice)
336 (lower panel). Data represent the mean ± SEM. **G)** Representative images of single muscle fibers
337 treated with GAP-SCR or GAP-REW from Wt mice after 96 hours in culture, incubated for 24 hours
338 with EdU (red). Nuclei were visualized with DAPI (blu) (upper panel); histograms represent the mean
339 of clusters (n>2), pairs (n=2) and single cells $PAX7^{+}$ (n=1) per fiber. Data represent the mean ± SEM
340 of 80 fibers per condition; n=5 mice (lower panel, right). The histogram (lower panel, left) shows the
341 number of Pax7+ cells per fiber (50 fibers per condition; n=5 mice). Data information: statistical

342 analysis was performed using unpaired Student's t-test: *P<0.05, **P<0.01, ***P<0.001.

343

344 **Figure 3: *Lnc-Rewind* and *Wnt7b* genes display opposite pattern of expression**

345 **A)** Schematic UCSC visualization showing the chromosome position and the lnc-Rewind
346 neighbouring genes. **B)** TSS usage analysis of Wnt7b, lnc-Rewind, Atxn10 and Cdpf1 performed by
347 using FANTOM5 (Phase1 and 2) CAGE datasets. Each bar represents the relative logarithmic
348 expression (rle) of the Tag Per Million (TPM) values of the TSS of each gene in one sample (1196
349 samples). The order of the samples is the same in each of the histograms. **C)** TPM expression (from
350 RNA-seq analysis) of lnc-Rewind neighbouring genes in GAP-SCR *versus* GAP-REW treated
351 MuSCs. TPM expression values are presented as an average±SD of 4 biological replicates. **D)** qRT-
352 PCR quantification of lnc-Rewind neighbouring genes in GAP-SCR *versus* GAP-REW treated
353 MuSCs. Data were normalized to GAPDH mRNA and represent the average ±SEM of 4 biological
354 replicates. Data information: *P<0.05, **P<0.01, paired Student's t-test.

355

356 **Figure 4: Lnc-Rewind directly interacts with the methyltransferase G9a and mediates specific**
357 ***in-cis* repression of *Wnt7b*.**

358 **A)** G9A and EZH2 native RNA immunoprecipitation (RIP) performed on nuclear extracts of C_2C_{12}
359 proliferating myoblasts. Data represent mean ±SEM of 4 biological replicates. Western blot analysis
360 of G9A and EZH2 (upper panel) and qRT-PCR quantification of lnc-Rewind recovery (lower panel)
361 are shown. Gapdh RNA serves as negative control. **B)** G9a Cross-linked RNA immunoprecipitation
362 (CLIP) performed on nuclear extracts of C_2C_{12} proliferating myoblasts. Data represent mean ±SEM
363 of 3 biological replicates. Western blot analysis of G9A (upper panel) and qRT-PCR quantification
364 of lnc-Rewind recovery (lower panel) are shown. Gapdh RNA and EZH2 protein serve as negative
365 controls; Kcnq1ot RNA was used as positive control. **C)** A zoom in into the genomic regions upstream
366 *Wnt7b* gene. Amplicons used to check the H3K9me2 epigenetic mark are shown. Chromatin
367 immunoprecipitation (ChIP) of H3K9me2, performed in Wt MuSCs upon lnc-Rewind

368 downregulation; MuSCs transfected with scrambled (GAP-SCR) gapmers have been used as control.
369 Enrichment is represented as percentage of input DNA (% input). Ube2b and R15 genomic regions
370 were used as negative and positive control, respectively. The graph shows the averaged value derived
371 from n=6 independent experiments. **D)** Proposed model for the murine lnc-Rewind mode of action in
372 muscle cells. In proliferating myoblasts, lnc-Rewind is expressed and guide the silencing
373 methyltransferase G9a on *Wnt7b* promoter to repress its transcription. Data information: *P<0.05,
374 paired Student's t-test.

375

376 **METHODS**

377 **Ethics statement and animal procedures**

378 For the experiments described in this study, C57/BL10 wild-type mice were used and differences
379 which were observed in both male and female mice were included in experiments. Animals were
380 treated in respect to housing, nutrition and care according to the guidelines of Good laboratory
381 Practice (GLP). All experimental protocols were approved and conformed to the regulatory standards.
382 All animals were kept in a temperature of 22°C ± 3°C with a humidity between 50% and 60%, in
383 animal cages with at least 5 animals.

384

385 **Cell preparation and FACS sorting**

386 Cell isolation and labeling was essentially performed as described in (Mozzetta, 2016). Isolation of
387 cells from two months old C57/Bl10 WT mice was performed as follows: briefly, whole lower
388 hindlimb muscles were carefully isolated, minced and digested in PBS (Sigma) supplemented with
389 2.4 U/ml Dispase II (Roche), 100 µg/ml Collagenase A (Roche), 50 mM CaCl2, 1 M MgCl2, 10
390 mg/ml DNase I (Roche) for 1 hour at 37 °C under agitation. Muscle slurries were passed 10 times
391 through a 20G syringe (BD Bioscience). Cell suspension was obtained after three successive cycles
392 of straining and washing in Washing Buffer consisting of HBSS containing 0.2% BSA (Sigma

393 Aldrich), 1% penicillin-streptomycin. Cells were incubated with primary antibodies CD31-PE
394 (MiltenyBiotec, 130111540), CD45- PE (MiltenyBiotec, 139110797), Ter119-PE (MiltenyBiotec,
395 130112909) 1:25; Sca1-FITC (MiltenyBiotec, 130116490) 1:25 e α7Integrin-APCVio770
396 (MiltenyBiotec, 130102719) 1:20 for 45 min on ice diluted in HBSS containing 0.2% BSA, 1%
397 penicillin-streptomycin and 1% DNAse I. The suspension was finally washed and resuspended in
398 PBS containing 2% Fetal Bovine Serum (FBS) and EDTA 0.5 μM. Cells were sorted using a
399 FACSAriaIII (Becton Dickinson, BD Biosciences) equipped with 488nm, 561nm and 633nm laser
400 and FACSDiva software (BD Biosciences version 6.1.3). Data were analyzed using a FlowJo
401 software (Tree Star, version 9.3.2). Briefly, cells were first gated based on morphology using forward
402 versus side scatter area parameter (FSC-A versus SSC-A) strategy followed by doublets exclusion
403 with morphology parameter area versus width (A versus W). Muscle satellite cells (MuSCs) were
404 isolated as $Ter119_{neg}/CD45_{neg}/CD31_{neg}/a7\text{-}integrin_{pos}/Sca1_{neg}$ cells (see **FigureS1C**, left and right
405 panels). To reduce stress, cells were isolated in gentle conditions using a ceramic nozzle of size
406 100μm, a low sheath pressure of 19.84 pound-force per square inch (psi) that maintain the sample
407 pressure at 18.96 psi and a maximum acquisition rate of 3000 events/s. Cells were collected in 5
408 polypropylene tubes. Following isolation, an aliquot of the sorted cells was evaluated for purity at the
409 same instrument resulting in an enrichment >98-99% (see **FigureS1C** right panel).
410

411 **Cell culture conditions and transfection**

412 Freshly sorted cells were plated on ECM Gel (Sigma)-coated dishes in Cyto-grow (Resnova)
413 complete medium as a growth medium (GM) and cultured at 37°C and 5% CO2. After 5 days in GM,
414 SCs were exposed, generally for 2 days, to differentiation medium (DM) consisting of DMEM with
415 5% Horse Serum (HS). Cells were counted on DAPI-stained images using the ImageJ tool "Multi
416 point". Downregulation of Lnc-Rewind expression was performed at ~50% confluence by transfection
417 in Lipofectamine 2000 (Invitrogen), with 75nM of LNA GapmeRs (Euroclone), according to

418 manufacturer's instructions. MuSCs were subjected to two consecutive (overnight) rounds of
419 transfection and harvested 24 hours after second transfection.
420 GapmeRs were designed against Lnc-Rewind sequence using the Exiqon web tool
421 (http://www.exiqon.com/ls/Pages). Negative Control A (Euroclone) was used as negative (Scramble)
422 control. Sequences are reported in Table S2
423 For EdU (Invitrogen) detection cells were incubated for 6h and stained using Click-iT™ EdU Alexa
424 Flour™ 594 HCS Assay (Invitrogen) according to the manufacturer's instructions.
425
426 **Single myofibers isolation and immunofluorescence**
427 Single myofibers were isolated from Extensor digitorum longus (EDL) muscles of C57/Bl10 mice
428 and digested in 2mg/ml Collagenase I (Sigma) for 1 h at 37 °C, gently shacked every 10 minutes.
429 Single fibers were obtained gently triturating the digested EDL muscles using a glass pipette in
430 DMEM supplemented with 10% HS (horse serum). The myofibers were manually collected under a
431 dissecting microscope and cultured in DMEM + Pyr with 20% FBS, 2,5 ng/ml FGF (Gibco) and 1%
432 Chick Embryo Extract (CEE) (Life Science Production). Downregulation of Lnc-Rewind expression
433 was performed 4 h after plating with one round of transfection, as described above. The fibers were
434 incubated for 24h with EdU (Invitrogen) and were analyzed 96h after plating.
435 For EdU detection cells were stained using Click-iT™ EdU Alexa Flour™ 594 HCS Assay
436 (Invitrogen) according to the manufacturer's instructions.
437 For the immunofluorescence, the single myofibers were fixed with 4% paraformaldehyde in PBS for
438 20 min at RT, permeabilized with 0.5% Triton X-100 in PBS, and blocked with 10% FBS in PBS for
439 1 h at RT. Primary antibodies (Pax7 (DSHB, Pax7-s) 1:10 and Ki67 (Abcam, ab15580) 1:100) were
440 diluted in 10%FBS-PBS and incubated overnight at 4°C. After incubation for 1h with the appropriate
441 secondary antibodies (Alexa Fluor 488 or 594 (Thermo Fisher)), nuclei were counterstained with
442 DAPI (Sigma) and fibers were mounted on cover-glasses. Images were taken with Axio Observer
443 microscope (ZEISS) and processed with ZEN 3.0 (Blue edition) software.

444

445 **RNA Imaging**

446 Lnc-Rewind *in situ* hybridization analyses were performed as previously described (Rossi et al.,
447 2019). Briefly, proliferating MuSC and C_2C_{12} cells were cultured on pre-coated glass coverslips and
448 then fixed in 4% paraformaldehyde/PBS (Electron Microscopy Sciences, Hatfield, PA). RNA
449 hybridization and signal development were carried out using Basescope assay (Advanced Cell
450 Diagnostics, Bio-Techne) and BA-Mm-lnc-Rewind probe-set (ref. 722581) designed to detect three
451 junction regions of Lnc-Rewind (exon/intron1, intron1/exon2, exon/intron2). A probe specific for
452 exon junction exon1/exon2 of human Dlc1 mRNA (BA-HS-DLC1, ref.716041) was used as negative
453 control. The images were collected as Z-stacks (200 nm Z-spacing) with MetaMorph software and
454 post-acquisition processing were performed by FIJI software to the entire image. 3D viewer plugin
455 was used to perform 3D-rendering.

456

457 **RNA analyses**

458 Total RNA from myoblasts/myotubes and MuSCs was extracted with TriReagent (Sigma). 0.5-1.0ug
459 of RNA were treated with RNase-free DNase I enzyme (Thermo scientific). Nucleus and Cytoplasmic
460 fractionations was performed using the Paris kit (Ambion, AM1921) according the protocol
461 specifications. RNA was reverse transcribed using the SuperScript VILO Master Mix (Thermo
462 Scientific). Real time quantitative PCRs were performed by using SYBR Green Master mix (Applied
463 Biosystems), according to the manufacturer's instructions. Relative expression values were
464 normalized to the housekeeping GAPDH transcript.

465

466 **Cell lysis and Immunoblot**

467 Total proteins were prepared by resuspending cells in RIPA buffer (50mM Tris-HCl pH 7.4, 150mM
468 NaCl, 0.1% SDS, 0.5% sodium deoxycholate, 1% NP-40, 1mM EDTA, protease and phosphatase
469 inhibitors (Roche)). Protein concentration was determined using a BCA assay (Thermo Fisher

470 Scientific). The cell lysate was denatured at 95 °C for 5 min. The cell lysates were resolved on 4%–
471 15% TGX gradient gels (Bio-Rad Laboratories) and transferred to nitrocellulose membrane
472 (Amersham). Membranes were blocked with 5% non-fat dried milk in TBS with 0.2% Tween for 1 h
473 at RT, and then incubated with primary antibody overnight at 4°C Primary antibodies used were
474 against: MF20 (MyHC) (DSHB, Mf20-s), G9a (Abcam, ab185050), Ezh2 (Cell Signaling, #3147),
475 Wnt7b (Abcam, ab94915), β-catenin (Santa Cruz biotechnology, sc-7963), Cyclin D3 (Santa Cruz
476 biotechnology, sc-182) and GAPDH (Sigma, G9545). After washing in TBS with 0.2% Tween,
477 membranes were incubated in HRP-conjugated specific secondary antibody (goat anti-rabbit-anti-
478 mouse (IgG-HRP Santa Cruz Biotechnologies)) for 1h at RT. After washing in TBS with 0.2%
479 Tween, blots were developed with Western lightning enhanced chemiluminescence (Thermo Fisher
480 Scientific), the signal detection was performed with the use of ChemiDoc (BioRad).
481
482 **RNA Immunoprecipitation (RIP)**
483 C_2C_{12} cells were washed with PBS and centrifuge at 2000 rpm for 5 minutes and resuspended in
484 Buffer A (20mM Tris HCl pH8.0, 10mM NaCl, 3mM MgCl2, 0.1% NP40, 10% Glicerol, 0.2mM
485 EDTA, 0.4mM PMSF, 1XPIC). In ice for 15 minutes and centrifuge at 2000 rpm for 5 minutes at
486 4°C to pellet the nuclei. The supernatant was collected as cytoplasmic extract. The pellet was re-
487 washed with buffer A for 3 times. The pellet was resuspended in NT2/Wash buffer (50mM Tris
488 pH7.4, 150mM NaCl, 1mM MgCl2, 0,5% NP40, 20mM EDTA, 1X PIC, 1X PMSF, 1 mM DTT),
489 break with 7mL dounce (thight pestel/B pestel) and centrifuged at 14000 rpm for 30 minutes at 4°C.
490 Protein A/G Magnetic beads (Thermos Scientific) were incubate with IgG, G9a (Abcam, ab185050)
491 and Ezh2 (Cell Signaling, #3147) antibody on rotating wheel ON at 4°C while the nuclear extract
492 was precleared with the beads. 10% of the nuclear extract was collected for INP. The NE was divided
493 in each sample with the coated beads (beads+ Ab) and incubate on rotating wheel ON at 4°C. The
494 beads were washed with NTS buffer and ¼ was collected for protein and ¾ for RNA analyses. RIP
495 qPCR results were represented as percentage of IP/input signal (% input).

496

497 **Cross-linking immunoprecipitation (CLIP) assay**

498 CLIP experiments were performed on nuclear extract obtained with some modification of the Rinn
499 et al. protocol (Rinn et al., 2007). Briefly, C_2C_{12} cells were washed with PBS and crosslinked with
500 UV rays and collected in Buffer A (20mM Tris HCl pH8.0, 10mM NaCl, 3mM MgCl2, 0.1% NP40,
501 10% Glicerol, 0.2mM EDTA, 0.4mM PMSF, 1XPIC). Cells were centrifuged at 500 xg for 10
502 minutes and resuspended in Buffer A, the nuclei pellet was resuspended in NP40 lysis buffer (50mM
503 HEPES-KOH, 150Mm KCL, 2Mm EDTA, 1Mm NaF, 0,5% NP40 PH 7.4, 0,5Mm DTT, 100X PIC).
504 Break with 7mL dounce (thight pestel/B pestel) and centrifuged at max speed for 20 minutes at 4°C.
505 The supernatant was quantified with bredford assay. 10% of the nuclear extract was collected for
506 INP. Protein A/G Magnetic beads (Thermos Scientific) were washed with PBS tween 0,02% (1X
507 PBS, 0,02% Tween-20) were incubate in PBS Tween 0,02% with IgG and G9a (Abcam, ab185050)
508 antibody on rotating wheel 1 h at RT. The NE was divided in each sample with the coated beads
509 (beads+ Ab) and incubate on rotating wheel ON at 4°C. The beads where washed 3 times with the
510 NP40 High Salt Buffer 0.5X (25 mM HEPES-KOH pH7.5, 250 mM KCL, 0.025% NP40), 2 times
511 with PNK Buffer (50mM Tris-HCL, 50Mm NaCl, 10mM MgCl2 pH7.5) and resuspended with NP40
512 lysis buffer. ¼ was taken for protein analysis where was add LSD 5X and DTT 100X, for 5 minutes
513 at 95°C. The rest was used for RNA analysis: the beads were resuspended in proteinase K buffer
514 (200MM Tris-HCL, 300 mM NaCl, 25 mM EDTA, 2%SDS pH 7.5).

515

516 **Chromatin Immunoprecipitation (ChIP)**

517 ChIP experiments were performed on chromatin extracts according to the manufacturer's protocol
518 (MAGnify ChIP; Life Technologies) by O.N. incubation with 3 µg of immobilized anti-H3K9me2
519 (Abcam ab1220) or rabbit IgG antibodies. A standard curve was generated for each primer pair testing
520 5-point dilutions of input sample. Fold enrichment was quantified using qRT-PCR (SYBR Green;
521 Qiagen) and calculated as a percentage of input chromatin (% Inp). Data from GAP-SCR *vs* GAP-

522 REW conditions represent the mean of six independent experiments ± SEM. Sequences of the
523 oligonucleotidies used for ChIP analyses are reported in Table S2.
524
525 **3'-end mRNA Sequencing and Bioinformatic analysis**
526 Total RNA was quantified using the Qubit 2.0 fluorimetric Assay (Thermo Fisher Scientific).
527 Libraries were prepared from 100 ng of total RNA using the QuantSeq 3' mRNA-Seq Library Prep
528 Kit FWD for Illumina (Lexogen GmbH); the quality was assessed by using screen tape High
529 sensitivity DNA D1000 (Agilent Technologies). Sequencing was performed on a NextSeq 500 using
530 a high-output single-end, 75 cycles, v2 Kit (Illumina Inc.). Illumina novaSeq base call (BCL) files
531 were converted in fastq file through bcl2fastq (version v2.20.0.422). Sequence reads were trimmed
532 using trimgalore (v0.4.1) to remove adapter sequences and low-quality end bases (regions with
533 average quality below Phred score 20). Alignment was performed with STAR 2.5.3a (Dobin et al.,
534 2013) on mm10 reference. The expression levels of genes were determined with htseq-count
535 0.9.1(Anders et al., 2015) by using mm10 Ensembl assembly (release 90). Genes having < 1 Count
536 Per Million (CPM) in at least 4 samples and those with a percentage of multi-mapping reads > 20%
537 were filtered out. Paired t-test was performed to select differentially expressed genes in GAP-REW
538 vs GAP-SCR conditions, setting 0.05 as p-value threshold. Gene ontology term enrichment analyses
539 were performed using GORILLA (Eden et al., 2009) providing the list of genes expressed in at least
540 one of the two conditions as background.
541 RNA-Seq reads from WT myoblasts cultured in growth medium (Legnini et al., 2017) were
542 downloaded from GEO (GSE70389), preprocessed using Trimmomatic 0.32 software (Bolger et al.,
543 2014) and aligned to human GRCh38 assembly using STAR 2.5.3a. The normalized read coverage
544 tracks (.tdf files) were created and loaded on IGV genome browser (Robinson et al., 2011).
545
546 **Table S2: List and sequences of the oligonucleotides and LNA gapmers used**

q-RTPCR	
lnc-REW FW	5'-tttcacttgctggcttttga-3'
lnc-REW RV	5'-actcccagccagctgtgtc-3'
lnc-REW EX3 FW	5'-ccccaggaaagtaagcacct-3'
lnc-REW Ex4 RV	5'-agagtcacccagggaagttg-3'
hslnc-REW FW	5'-caggtcacgatcgggttcac-3'
hslnc-REW RV	5'-gatgggctcctgatgtctcg-3'
GAPDH FW	5'-tgacgtgccgcctggagaaa-3'
GAPDH RV	5'-agtgtagcccaagatgcccttcag-3'
pre-GAPDH FW	5'-ggctcatggtatgtaggcagt-3'
pre-GAPDH RV	5'-gaaaacacgggggcaatgagt-3'
hsGAPDH FW	5'-ggaaggtgaaggtcggagtc-3'
hsGAPDH RV	5'-ttaccagagttaaaagcagccc-3'
MyoG FW	5'-tcccaacccaggagatcatt-3'
MyoG RV	5'-catatcctccaccgtgatgc-3'
MCK FW	5'-ttacactctgcctccgcact-3'
MCK RV	5'-gtacttgcccttgaactcgc-3'
miR-Let7-b	Qiagen Cat. No MS00003122
miR-Let7-c	Qiagen Cat. No 218300
Fam19a5 FW	5'-tcctcgtcctggtgattcac-3'
Fam19a5 RV	5'-ccggtctagggtcacaatct-3'
Tbc1d22a FW	5'-gaagcagttctggaagcgc-3'
Tbc1d22a RV	5'-gtgccatgtaacagcggatc-3'
Cerk FW	5'-gtttgtgcccactgttgagt-3'
Cerk RV	5'-ctggtatcgaccccaatcac-3'
Gramd4 FW	5'-agagttggccccgatcatc-3'
Gramd4 RV	5'-catgttcagcacggcactc-3'
Trmu FW	5'-gctgtggacaatcttggagc-3'
Trmu RV	5'-cgtcaggcttcttagtgtgc-3'
Gtse1 FW	5'-aaccccaaagttctcacgga-3'

Gtse1 RV	5'-gtagtccctgatgagcgtct-3'
Cdpf1 FW	5'-cgtttgagtgccagctttgt-3'
Cdpf1 RV	5'-agaaacctggccttgtctga-3'
Atxn10 FW	5'-cgatcggagttgctgttgat-3'
Atxn10 RV	5'-gccacatcgaaaagctgtca-3'
Fbln1 FW	5'-agagcggcttcatacaggat-3'
Fbln1 RV	5'-cttctggcatgtgtaggagc-3'
Fam118a FW	5'-cggaggaaggtgatgaagga-3'
Fam118a RV	5'-ccaagctgtcaaacacctcc-3'
Nup50 FW	5'-ggaacattctcagtggccag-3'
Nup50 RV	5'-ggctcctccgctatcagatt-3'
Prr5 FW	5'-gggcatggtgattcttcgtg-3'
Prr5 RV	5'-aagaaatcccaggtctccgc-3'
Parvb FW	5'-gaggagcgtaccatgatcga-3'
Parvb RV	5'-gcacatcgttgatccagtcc-3'
Samm50 FW	5'-ggaagccgagtttgtggaag-3'
Samm50 RV	5'-atccttagtccgcccaagtc-3'
Ttll12 FW	5'-cagagcgactatggggcc-3'
Ttll12 RV	5'-cacctcctccacctgcatta-3'
Kcnq1ot1 FW	5'-ctgttccctagagcttgccc-3'
Kcnq1ot1 RV	5'-tggttaatcctgcctgcctg-3'
Wnt7b FW	5'-accttcacaacaatgaggcg-3'
Wnt7b RV	5'-cttcatgcggtcctccagaa-3'
Ube2b FW	5'-GCCGAACTTGAAACTAGCGAC-3'
Ube2b RV	5'-GTTGCTTGCGGGCAACTACG-3'
R15 FW	5'-GTTTTTCATCGGACGGTGGC-3'
R15 RV	5'-CCGCCGCTCATACACCATAA-3'
G9a/91 FW	5'-AGGGGCAGATTTTGGACTCT-3'
G9a/91 RV	5'-CCCCATGAGTCATCCCTAGA-3'
G9a/93 FW	5'-AGCAACCACTAACTGCACTGT-3'

G9a/93 RV	5'-TGGCTGGATGATGGATAGAT-3'
G9a/94 FW	5'-AGCCAGAGCTTTGTGTAGGC-3'
G9a/94 RV	5'-CAGGATCCAAGCCAAGATTT-3'
G9a/95 FW	5'-TACCAGCACTGCTTCTGTGG-3'
G9a/95 RV	5'-TGCTAACTTCCCACCCTTTG-3'
LNA GAPmers	
GAP-SCR	Negative control A exiqon cat. n.300610
GAP-REW_1	5'-atcttggatctagcta-3'
GAP-REW_2	5'-gagctggtgatgaatg-3'
GAP-REW_3	5'-gaagagagtggtgaag-3'

547

548 **SUPPLEMENTAL EXPERIMENTAL PROCEDURES**

Figure S1. Related to Figure 1

A

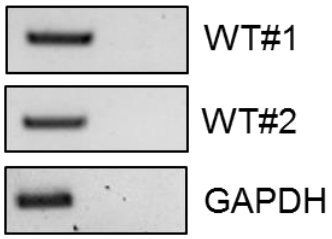

B

	Exonic Sequences	Intronic Sequences
Length	7501	28696
Sequence identity	3315/7501 (**44.2%**)	13493/28696 (**47.0%**)
Gaps	2730/7501 (36.4%)	11644/28696 (40.6%)
Score	15264.0	28625.5

C

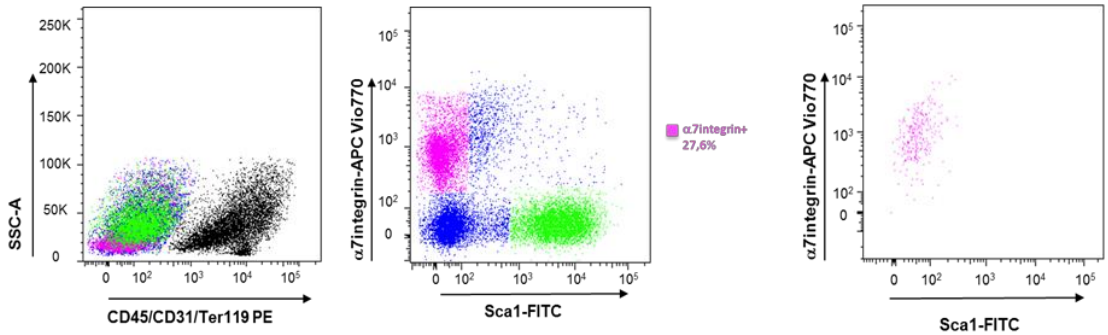

D

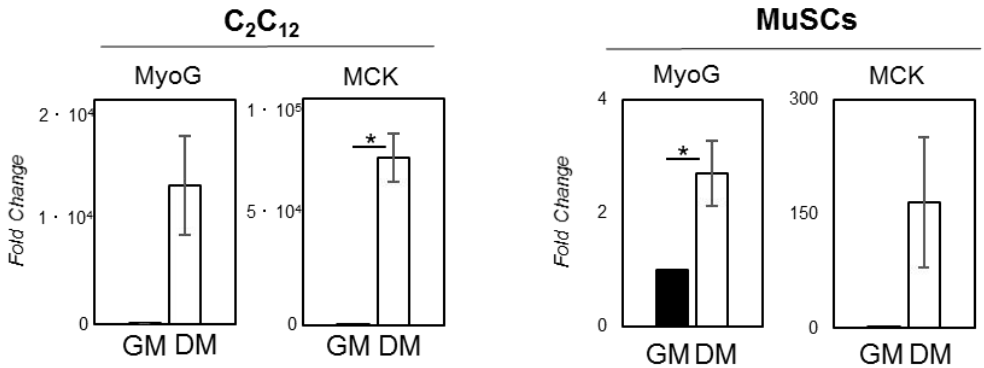

E

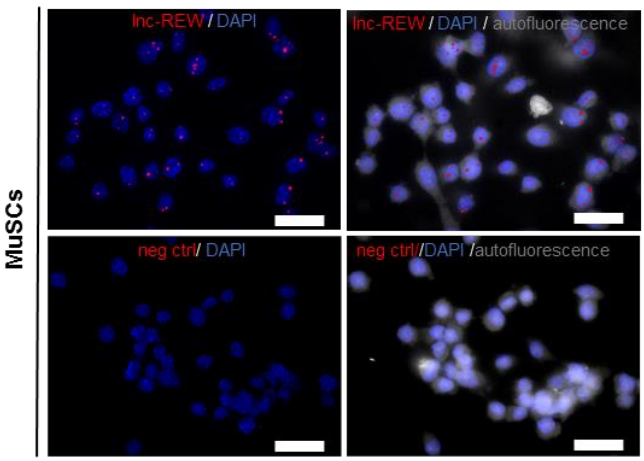

F

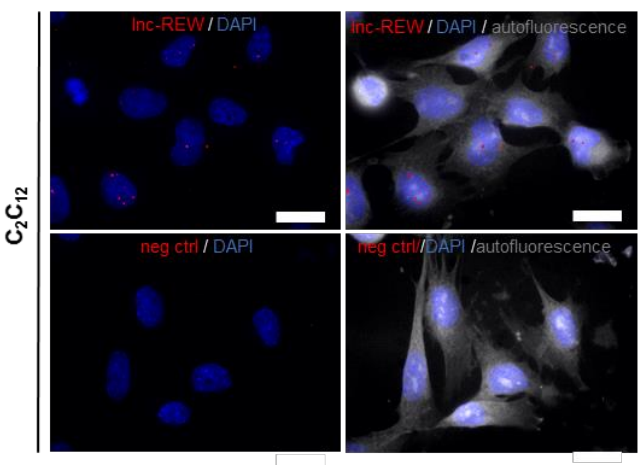

549

550 **Figure S1**

551 **A)** sqRT-PCR quantification of hs_lnc-Rewind in two different proliferating human myoblasts from
552 healthy donors in proliferating condition. Mature GAPDH was used as an amplification control. **B)**
553 Table represents the values obtained by analysing the local sequence alignment between the human
554 and murine lnc-Rewind transcripts. Data were produced by using the implementation of the Smith-
555 Waterman algorithm available at http://www.ebi.ac.uk/Tools/psa/emboss_water/. **C)** In WT mice,
556 lineage negative CD45/CD31/Ter119 PE cells were sorted for muscle stem cells based on
557 α7integrin expression (APC Vio770 positive cells, magenta) (left and middle panels). The check
558 purity plot shows the pureness of the sample (right panel). **D)** qRT-PCR quantification of MyoG and
559 MCK in C_2C_{12} and MuSCs in growth and differentiated conditions. Data represent the mean ±
560 SEM of 3 biological replicates and were normalised on Gapdh mRNA. **E)** Representative 60X
561 confocal images of MuSC cell cultures hybridized with probes set specific for lnc-Rewind and for a
562 human mRNA (dlc1). Autofluorescence (grey) is shown with false colour to visualize the cell body.
563 DAPI, 4',6-diamidino-2-phenylindole (blue); Scale bar: 25 um. **F)** Representative 60X confocal
564 images of C_2C_{12} cell cultures hybridized with probes set specific for lnc-Rewind and for a human
565 mRNA (dlc1). Autofluorescence (grey) is shown with false colour to visualize the cell body. DAPI,
566 4',6-diamidino-2-phenylindole (blue); Scale bar: 25 um. Data information: *P<0.05, paired
567 Student's t-test

Figure S2. Related to Figure 2 and Figure 3:

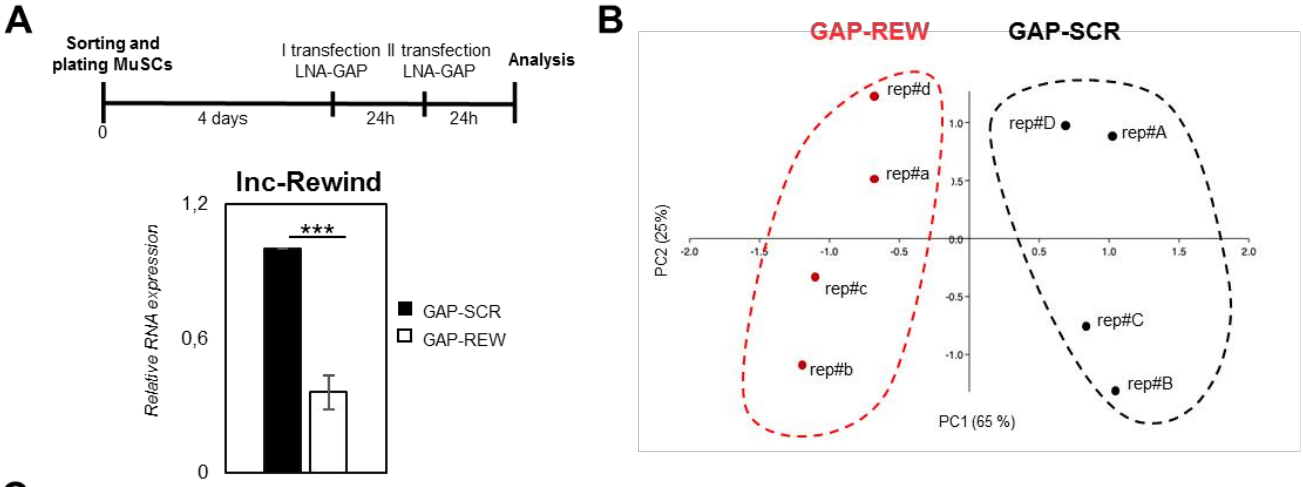

C

GO term	Description	P-value	FDR	Enrichment
GO:0003012	muscle system process	3.45E-7	4.74E-3	2.70
GO:0006941	striated muscle contraction	4.63E-7	3.18E-3	3.74
GO:0006936	muscle contraction	7.87E-7	3.6E-3	2.89
GO:0003009	skeletal muscle contraction	4.23E-6	1.45E-2	5.35
GO:0030111	regulation of Wnt signaling pathway	5.44E-4	1E0	1.83
GO:0030832	regulation of actin filament length	7.68E-4	1E0	2.00
GO:0006091	generation of precursor metabolites and energy	8.18E-4	1E0	1.83

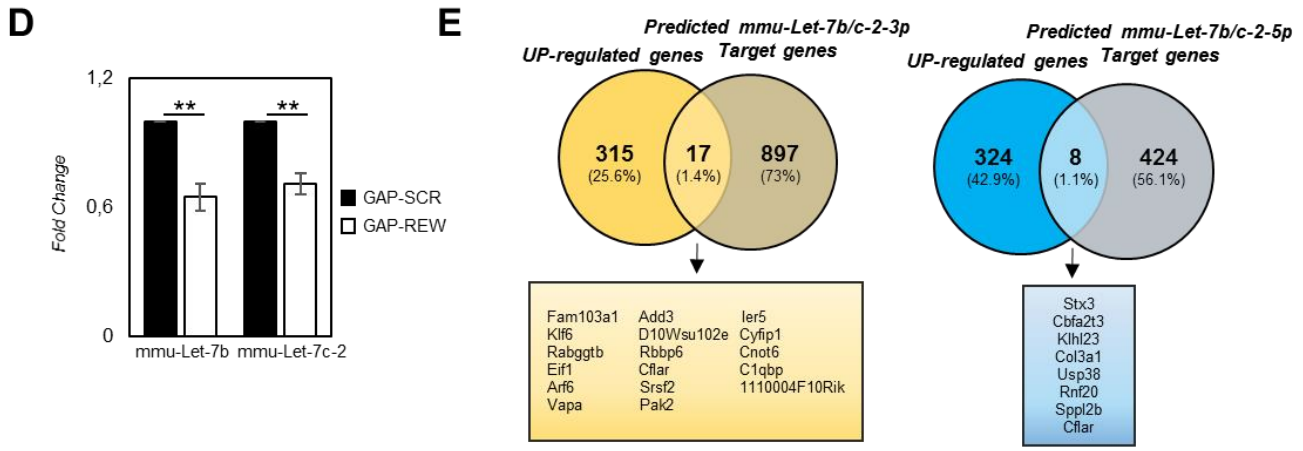

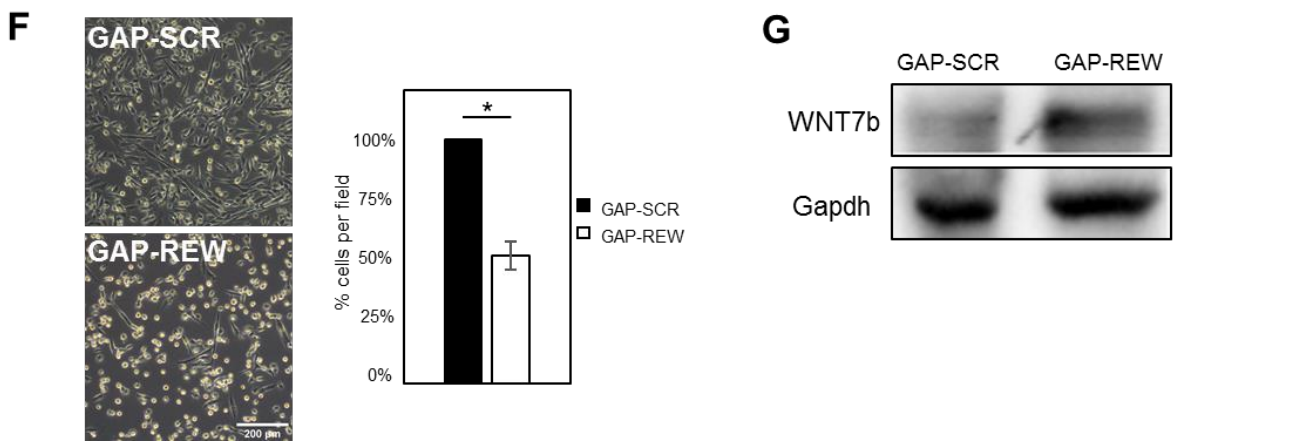

568

569 **Figure S2**

570 **A)** Schematic representation of the experimental condition of MuSCs treated with GAP-SCR or
571 GAP-REW (upper part). Real-time qRT-PCR quantification of lnc-Rewind in MuSCs treated with
572 GAP-SCR or GAP-REW. Data were normalized to Gapdh mRNA and represent the mean ± SEM
573 of n=4 biological replicates (lower part). **B)** PCA analysis of DEGs upon lnc-Rewind depletion.
574 GAP-SCR and GAP-REW treated samples replicates are shown respectively as red and black dots
575 (left panel). The plot represents each Eingvalue % for the different Principal components (right
576 panel). As shown in both panels, PCA1 and PCA2 represent the top two dimensions of the DEGs
577 which account respectively for 65%, 25% of the total variability. **C)** Table shows the GO terms,
578 their description, the p-value, the FDR (represented in decreasing order of statistical significance)
579 and the enrichment of the different categories showed in Figure 2C. **D)** Real-time qRT-PCR
580 quantification of mmu-Let7-b and mmu-Let7-c-2 in MuSCs treated with GAP-SCR or GAP-REW.
581 Data were normalized to Gapdh mRNA and represent the mean ± SEM of n=3 biological replicates.
582 **E)** Target prediction analysis performed by crossing the lnc-REW up-regulated genes with the
583 mmu-Let7-3p (yellow) and mmu-Let7-5p (Blue) predicted target genes. The predictions were
584 obtained from Targetscan database (Agarwal et al., 2015). **F)** Representative images (left) and cells
585 number quantification (right) of MuSCs treated with GAP-SCR or GAP-REW. Data represent the
586 mean ± SEM from 3 biological replicates. **G)** Western blot analysis performed on protein extracts
587 from MuSCs treated with GAP-SCR or GAP-RE. Data information: *P<0.05, **P<0.01,
588 ***P<0.001, paired Student's t-test

Figure S3. Related to Figure 4

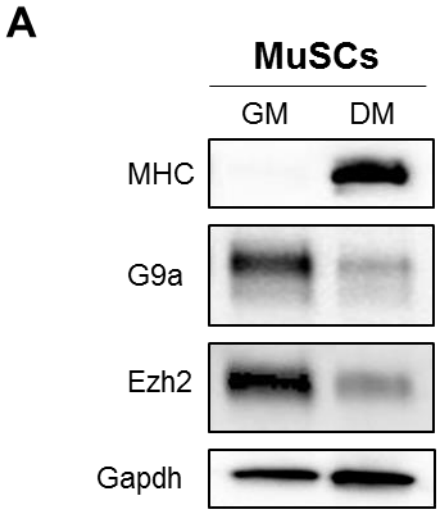

Figure S3

A) Western blot analysis performed on protein extracted from wild type MuSCs grown in growth (GM) and differentiated (DM) conditions.

REFERENCES

Abugessaisa, I., Noguchi, S., Hasegawa, A., Harshbarger, J., Kondo, A., Lizio, M., Severin, J., Carninci, P., Kawaji, H., and Kasukawa, T. (2017). FANTOM5 CAGE profiles of human and mouse reprocessed for GRCh38 and GRCm38 genome assemblies. Sci Data *4*, 170107.

Anders, S., Pyl, P.T., and Huber, W. (2015). HTSeq--a Python framework to work with high-throughput sequencing data. Bioinformatics *31*, 166-169.

Babicki, S., Arndt, D., Marcu, A., Liang, Y., Grant, J.R., Maciejewski, A., and Wishart, D.S. (2016). Heatmapper: web-enabled heat mapping for all. Nucleic Acids Res *44*, W147-153.

Ballarino, M., Cazzella, V., D'Andrea, D., Grassi, L., Bisceglie, L., Cipriano, A., Santini, T., Pinnaro, C., Morlando, M., Tramontano, A., *et al*. (2015). Novel long noncoding RNAs (lncRNAs) in myogenesis: a miR-31 overlapping lncRNA transcript controls myoblast differentiation. Mol Cell Biol *35*, 728-736.

Ballarino, M., Morlando, M., Fatica, A., and Bozzoni, I. (2016). Non-coding RNAs in muscle differentiation and musculoskeletal disease. J Clin Invest *126*, 2021-2030.

Batista, P.J., and Chang, H.Y. (2013). Long noncoding RNAs: cellular address codes in development and disease. Cell *152*, 1298-1307.

Bolger, A.M., Lohse, M., and Usadel, B. (2014). Trimmomatic: a flexible trimmer for Illumina sequence data. Bioinformatics *30*, 2114-2120.

Brack, A.S., Conboy, I.M., Conboy, M.J., Shen, J., and Rando, T.A. (2008). A temporal switch from notch to Wnt signaling in muscle stem cells is necessary for normal adult myogenesis. Cell Stem Cell *2*, 50-59.

Caretti, G., Di Padova, M., Micales, B., Lyons, G.E., and Sartorelli, V. (2004). The Polycomb Ezh2 methyltransferase regulates muscle gene expression and skeletal muscle differentiation. Genes Dev *18*, 2627-2638.

618 Carlevaro, G., Lantos, A.B., Canepa, G.E., de Los Milagros Camara, M., Somoza, M., Buscaglia,
619 C.A., Campetella, O., and Mucci, J. (2019). Metabolic Labeling of Surface Neo-sialylglyconjugates
620 Catalyzed by Trypanosoma cruzi trans-Sialidase. Methods Mol Biol *1955*, 135-146.
621 Carninci, P., Kasukawa, T., Katayama, S., Gough, J., Frith, M.C., Maeda, N., Oyama, R., Ravasi,
622 T., Lenhard, B., Wells, C., *et al*. (2005). The transcriptional landscape of the mammalian genome.
623 Science *309*, 1559-1563.
624 Chen, J., Tu, X., Esen, E., Joeng, K.S., Lin, C., Arbeit, J.M., Ruegg, M.A., Hall, M.N., Ma, L., and
625 Long, F. (2014). WNT7B promotes bone formation in part through mTORC1. PLoS Genet *10*,
626 e1004145.
627 Cipriano, A., and Ballarino, M. (2018). The Ever-Evolving Concept of the Gene: The Use of
628 RNA/Protein Experimental Techniques to Understand Genome Functions. Front Mol Biosci *5*, 20.
629 Dobin, A., Davis, C.A., Schlesinger, F., Drenkow, J., Zaleski, C., Jha, S., Batut, P., Chaisson, M.,
630 and Gingeras, T.R. (2013). STAR: ultrafast universal RNA-seq aligner. Bioinformatics *29*, 15-21.
631 Eden, E., Navon, R., Steinfeld, I., Lipson, D., and Yakhini, Z. (2009). GOrilla: a tool for discovery
632 and visualization of enriched GO terms in ranked gene lists. BMC Bioinformatics *10*, 48.
633 Eliazer, S., Muncie, J.M., Christensen, J., Sun, X., D'Urso, R.S., Weaver, V.M., and Brack, A.S.
634 (2019). Wnt4 from the Niche Controls the Mechano-Properties and Quiescent State of Muscle Stem
635 Cells. Cell Stem Cell.
636 Engreitz, J.M., Haines, J.E., Perez, E.M., Munson, G., Chen, J., Kane, M., McDonel, P.E., Guttman,
637 M., and Lander, E.S. (2016). Local regulation of gene expression by lncRNA promoters,
638 transcription and splicing. Nature *539*, 452-455.
639 Fatica, A., and Bozzoni, I. (2014). Long non-coding RNAs: new players in cell differentiation and
640 development. Nat Rev Genet *15*, 7-21.
641 Figeac, N., and Zammit, P.S. (2015). Coordinated action of Axin1 and Axin2 suppresses beta-
642 catenin to regulate muscle stem cell function. Cell Signal *27*, 1652-1665.
643 Guttman, M., and Rinn, J.L. (2012). Modular regulatory principles of large non-coding RNAs.
644 Nature *482*, 339-346.
645 Hu, P., Chu, J., Wu, Y., Sun, L., Lv, X., Zhu, Y., Li, J., Guo, Q., Gong, C., Liu, B., *et al*. (2015).
646 NBAT1 suppresses breast cancer metastasis by regulating DKK1 via PRC2. Oncotarget *6*, 32410-
647 32425.
648 Huarte, M., Guttman, M., Feldser, D., Garber, M., Koziol, M.J., Kenzelmann-Broz, D., Khalil,
649 A.M., Zuk, O., Amit, I., Rabani, M., *et al*. (2010). A large intergenic noncoding RNA induced by
650 p53 mediates global gene repression in the p53 response. Cell *142*, 409-419.
651 Khalil, A.M., Guttman, M., Huarte, M., Garber, M., Raj, A., Rivea Morales, D., Thomas, K.,
652 Presser, A., Bernstein, B.E., van Oudenaarden, A., *et al*. (2009). Many human large intergenic
653 noncoding RNAs associate with chromatin-modifying complexes and affect gene expression. Proc
654 Natl Acad Sci U S A *106*, 11667-11672.
655 Kopp, F., and Mendell, J.T. (2018). Functional Classification and Experimental Dissection of Long
656 Noncoding RNAs. Cell *172*, 393-407.
657 Lacour, F., Vezin, E., Bentzinger, C.F., Sincennes, M.C., Giordani, L., Ferry, A., Mitchell, R.,
658 Patel, K., Rudnicki, M.A., Chaboissier, M.C., *et al*. (2017). R-spondin1 Controls Muscle Cell
659 Fusion through Dual Regulation of Antagonistic Wnt Signaling Pathways. Cell Rep *18*, 2320-2330.
660 Le Grand, F., Jones, A.E., Seale, V., Scime, A., and Rudnicki, M.A. (2009). Wnt7a activates the
661 planar cell polarity pathway to drive the symmetric expansion of satellite stem cells. Cell Stem Cell
662 *4*, 535-547.
663 Legnini, I., Di Timoteo, G., Rossi, F., Morlando, M., Briganti, F., Sthandier, O., Fatica, A., Santini,
664 T., Andronache, A., Wade, M., *et al*. (2017). Circ-ZNF609 Is a Circular RNA that Can Be
665 Translated and Functions in Myogenesis. Mol Cell *66*, 22-37 e29.
666 Ling, B.M., Bharathy, N., Chung, T.K., Kok, W.K., Li, S., Tan, Y.H., Rao, V.K., Gopinadhan, S.,
667 Sartorelli, V., Walsh, M.J., *et al*. (2012). Lysine methyltransferase G9a methylates the transcription
668 factor MyoD and regulates skeletal muscle differentiation. Proc Natl Acad Sci U S A *109*, 841-846.

669 Lu, L., Sun, K., Chen, X., Zhao, Y., Wang, L., Zhou, L., Sun, H., and Wang, H. (2013). Genome-
670 wide survey by ChIP-seq reveals YY1 regulation of lincRNAs in skeletal myogenesis. EMBO J *32*,
671 2575-2588.
672 Maamar, H., Cabili, M.N., Rinn, J., and Raj, A. (2013). linc-HOXA1 is a noncoding RNA that
673 represses Hoxa1 transcription in cis. Genes Dev *27*, 1260-1271.
674 McHugh, C.A., Chen, C.K., Chow, A., Surka, C.F., Tran, C., McDonel, P., Pandya-Jones, A.,
675 Blanco, M., Burghard, C., Moradian, A., *et al*. (2015). The Xist lncRNA interacts directly with
676 SHARP to silence transcription through HDAC3. Nature *521*, 232-236.
677 Mozzetta, C. (2016). Isolation and culture of muscle stem cells, Vol 1480.
678 Mozzetta, C., Boyarchuk, E., Pontis, J., and Ait-Si-Ali, S. (2015). Sound of silence: the properties
679 and functions of repressive Lys methyltransferases. Nat Rev Mol Cell Biol *16*, 499-513.
680 Nagano, T., Mitchell, J.A., Sanz, L.A., Pauler, F.M., Ferguson-Smith, A.C., Feil, R., and Fraser, P.
681 (2008). The Air noncoding RNA epigenetically silences transcription by targeting G9a to
682 chromatin. Science *322*, 1717-1720.
683 Noguchi, S., Arakawa, T., Fukuda, S., Furuno, M., Hasegawa, A., Hori, F., Ishikawa-Kato, S.,
684 Kaida, K., Kaiho, A., Kanamori-Katayama, M., *et al*. (2017). FANTOM5 CAGE profiles of human
685 and mouse samples. Sci Data *4*, 170112.
686 Nusse, R., and Clevers, H. (2017). Wnt/beta-Catenin Signaling, Disease, and Emerging Therapeutic
687 Modalities. Cell *169*, 985-999.
688 Ong, M.S., Cai, W., Yuan, Y., Leong, H.C., Tan, T.Z., Mohammad, A., You, M.L., Arfuso, F.,
689 Goh, B.C., Warrier, S., *et al*. (2017). 'Lnc'-ing Wnt in female reproductive cancers: therapeutic
690 potential of long non-coding RNAs in Wnt signalling. Br J Pharmacol *174*, 4684-4700.
691 Pandey, R.R., Mondal, T., Mohammad, F., Enroth, S., Redrup, L., Komorowski, J., Nagano, T.,
692 Mancini-Dinardo, D., and Kanduri, C. (2008). Kcnq1ot1 antisense noncoding RNA mediates
693 lineage-specific transcriptional silencing through chromatin-level regulation. Mol Cell *32*, 232-246.
694 Pang, K.C., Frith, M.C., and Mattick, J.S. (2006). Rapid evolution of noncoding RNAs: lack of
695 conservation does not mean lack of function. Trends Genet *22*, 1-5.
696 Parisi, A., Lacour, F., Giordani, L., Colnot, S., Maire, P., and Le Grand, F. (2015). APC is required
697 for muscle stem cell proliferation and skeletal muscle tissue repair. J Cell Biol *210*, 717-726.
698 Polesskaya, A., Seale, P., and Rudnicki, M.A. (2003). Wnt signaling induces the myogenic
699 specification of resident CD45+ adult stem cells during muscle regeneration. Cell *113*, 841-852.
700 Rinn, J.L., and Chang, H.Y. (2012). Genome regulation by long noncoding RNAs. Annu Rev
701 Biochem *81*, 145-166.
702 Rinn, J.L., Kertesz, M., Wang, J.K., Squazzo, S.L., Xu, X., Brugmann, S.A., Goodnough, L.H.,
703 Helms, J.A., Farnham, P.J., Segal, E., *et al*. (2007). Functional demarcation of active and silent
704 chromatin domains in human HOX loci by noncoding RNAs. Cell *129*, 1311-1323.
705 Robinson, J.T., Thorvaldsdottir, H., Winckler, W., Guttman, M., Lander, E.S., Getz, G., and
706 Mesirov, J.P. (2011). Integrative genomics viewer. Nat Biotechnol *29*, 24-26.
707 Rossi, F., Legnini, I., Megiorni, F., Colantoni, A., Santini, T., Morlando, M., Di Timoteo, G.,
708 Dattilo, D., Dominici, C., and Bozzoni, I. (2019). Circ-ZNF609 regulates G1-S progression in
709 rhabdomyosarcoma. Oncogene *38*, 3843-3854.
710 Rudolf, A., Schirwis, E., Giordani, L., Parisi, A., Lepper, C., Taketo, M.M., and Le Grand, F.
711 (2016). beta-Catenin Activation in Muscle Progenitor Cells Regulates Tissue Repair. Cell Rep *15*,
712 1277-1290.
713 Shen, P., Pichler, M., Chen, M., Calin, G.A., and Ling, H. (2017). To Wnt or Lose: The Missing
714 Non-Coding Linc in Colorectal Cancer. Int J Mol Sci *18*.
715 Sun, Q., Hao, Q., and Prasanth, K.V. (2018). Nuclear Long Noncoding RNAs: Key Regulators of
716 Gene Expression. Trends Genet *34*, 142-157.
717 Ulitsky, I., and Bartel, D.P. (2013). lincRNAs: genomics, evolution, and mechanisms. Cell *154*, 26-
718 46.

von Maltzahn, J., Chang, N.C., Bentzinger, C.F., and Rudnicki, M.A. (2012). Wnt signaling in myogenesis. Trends Cell Biol *22*, 602-609.

Wang, K.C., Yang, Y.W., Liu, B., Sanyal, A., Corces-Zimmerman, R., Chen, Y., Lajoie, B.R., Protacio, A., Flynn, R.A., Gupta, R.A., *et al*. (2011). A long noncoding RNA maintains active chromatin to coordinate homeotic gene expression. Nature *472*, 120-124.

Wang, L., Zhao, Y., Bao, X., Zhu, X., Kwok, Y.K., Sun, K., Chen, X., Huang, Y., Jauch, R., Esteban, M.A., *et al*. (2015). LncRNA Dum interacts with Dnmts to regulate Dppa2 expression during myogenic differentiation and muscle regeneration. Cell Res *25*, 335-350.

Wang, Z., Shu, W., Lu, M.M., and Morrisey, E.E. (2005). Wnt7b activates canonical signaling in epithelial and vascular smooth muscle cells through interactions with Fzd1, Fzd10, and LRP5. Mol Cell Biol *25*, 5022-5030.

Zarkou, V., Galaras, A., Giakountis, A., and Hatzis, P. (2018). Crosstalk mechanisms between the WNT signaling pathway and long non-coding RNAs. Noncoding RNA Res *3*, 42-53.

Zhao, J., Sun, B.K., Erwin, J.A., Song, J.J., and Lee, J.T. (2008). Polycomb proteins targeted by a short repeat RNA to the mouse X chromosome. Science *322*, 750-756.

Zhao, Y., Chen, M., Lian, D., Li, Y., Li, Y., Wang, J., Deng, S., Yu, K., and Lian, Z. (2019). Non-Coding RNA Regulates the Myogenesis of Skeletal Muscle Satellite Cells, Injury Repair and Diseases. Cells *8*.

Zhu, M., Liu, J., Xiao, J., Yang, L., Cai, M., Shen, H., Chen, X., Ma, Y., Hu, S., Wang, Z., *et al*. (2017). Lnc-mg is a long non-coding RNA that promotes myogenesis. Nat Commun *8*, 14718.